

INTERSEISMIC AND LONG-TERM DEFORMATION OF SOUTHEASTERN SICILY DRIVEN BY THE IONIAN SLAB ROLL-BACK

Amélie Viger^{1*}, Stéphane Dominguez^{1*}, Stéphane Mazzotti¹,
Michel Peyret¹, Maxime Henriquet², Giovanni Barreca^{3*},
Carmelo Monaco³, Adrien Damon¹

April 17, 2024

1 1. [Montpellier Université - CNRS, Géosciences Montpellier, France](#)

2 2. Aix-Marseille Université, CEREGE, Aix-en-Provence, France

3 3. [Università di Catania](#), Dipartimento di Scienze Biologiche, Geologiche e Ambientali, Sezione
4 di Science della Terra, Italy

5 * e-mail, amelie.viger.geo@gmail.com, stephane.dominguez@umontpellier.fr, giobarre@unict.it

6 Key Points

- 7 • Recent satellite geodetic data shed new light on the origin of the active deformations
8 affecting Southeastern Sicily.
- 9 • Several deformation processes, including crustal flexure and faulting, are investi-
10 gated to determine the most reliable mechanical explanation.
- 11 • Seismic cycle, surface, and crustal deformations of Southeastern Sicily are mainly
12 driven by the southward migration of the Ionian slab roll-back.

13 Abstract:

14 New satellite geodetic data challenge our knowledge of the deformation mech-
15 anisms driving the active deformations affecting Southeastern Sicily. The PS-InSAR
16 measurements evidence a generalized subsidence and an eastward tilting of the Hyblean
17 Plateau combined with a local relative uplift along its eastern coast. To find a me-
18 chanical explanation for the present-day strain field, we investigate short and large-scale
19 surface-to-crustal deformation processes. Geological and geophysical data suggest that
20 the southward migration of the Calabrian subduction could be the causative geodynamic

21 process. We evaluate this hypothesis using flexural modeling and show that **the com-**
22 **bin**ed downward pull force, induced by the Ionian slab roll-back, and the overloading of
23 **the Calabrian accretionary prism, is strong enough to flex** the adjacent Hyblean continen-
24 tal **domain**, explaining the measured large-scale subsidence and eastward bending of the
25 Hyblean Plateau. To explain the short-scale relative uplift evidenced along the eastern
26 coast, we perform elastic modeling on identified or inferred onshore and offshore normal
27 faults. We also investigate the potential effects of other deformation processes including
28 upwelling mantle flow, volcanic deflation, and hydrologic loading. Our results enable us
29 to propose an original seismic cycle model for Southeastern Sicily, linking the current
30 interseismic strain field **with** available long-term deformation data. This model is mainly
31 driven by the southward migration of the Ionian slab roll-back which induces a downward
32 force capable **of flexuring** the Hyblean crust.

33

34 **Keywords:** Southeastern Sicily, surface deformation, PS-InSAR, slab roll-back, slab pull,
35 crustal/lithospheric flexure, extrado faulting, seismic cycle, numerical modeling

36

37 1 Introduction

38 Geodetic measurements, instrumental seismicity, onshore/offshore geology, and
39 geophysics, all indicate that Southeastern Sicily is actively deforming (e.g., Azzaro and
40 Barbano, 2000; Mastrolembo et al., 2014; Meschis et al., 2020; Anzidei et al., 2021). This
41 region also suffered the most powerful and devastating earthquake, the 1693 Mw \sim 7.4
42 Val-di-Noto earthquake, reported in **the Italian seismicity catalog**. **This earthquake is**
43 **thought to have** occurred **offshore** the eastern margin of the Hyblean Plateau, **triggering**
44 **a widespread tsunami** (e.g., Azzaro and Barbano, 2000; Gutscher et al., 2006; Scicchitano
45 et al., 2022). The current geologic and tectonic framework is in line with the Cenozoic
46 geodynamic evolution of the Central Mediterranean (Figure 1), but also appears to be
47 influenced by the Mesozoic pre-structuration of this region (e.g., Carminati and Doglioni,
48 2005; Frizon De Lamotte et al., 2011; Henriquet et al., 2020; Van Hinsbergen et al., 2020).
49 In the Late Cretaceous (~~\sim 80 Myr~~), the Africa/Eurasia plates convergence initiated the
50 subduction of the Alpine Tethys under the Apulia-Adria **and Iberia plates, giving rise to**

51 the Alpine orogeny (e.g., Handy et al., 2010, 2015; Van Hinsbergen et al., 2020; Jolivet,
52 2023). During the early Cenozoic, the ~~Alpine-Tethys~~ subduction ~~has~~ experienced polarity
53 reversal (e.g., Handy et al., 2010; Almeida et al., 2022) followed by, since at least the
54 Oligocene, long-lasting slab roll-back, causing the drifting of continental micro-blocks,
55 detached from the Iberian margin and the opening of back-arc basins throughout the
56 Mediterranean realm (e.g., Gueguen et al., 1998; Faccenna et al., 2001; Rosenbaum et al.,
57 2002; Carminati et al., 2012; Van Hinsbergen et al., 2020). During the Mio-Pliocene
58 (10-5 Myr), the collision between the southeastward migrating Calabrian-Peloritan Arc,
59 and associated Calabrian Accretionary Prism (CAP), with the Northern African passive
60 margin led to the formation of the Sicilian fold-and-thrust belt (e.g., Gueguen et al.,
61 1998; Henriquet et al., 2020). During the Plio-Pleistocene (5-2 Myr), the Calabrian Arc
62 and the retreating Ionian slab continued strongly interacting with the crustal structure
63 of the African margin, particularly with the thick Pelagian continental Platform and the
64 Malta Escarpment (Wortel and Spakman, 2000) (Figure 1). These ~~three~~ major tectonic
65 domains, which originated during the Triassic period, were shaped by the fragmentation
66 of the Pangea in the early Jurassic, leading to the opening of the Neo-Tethys Ocean (e.g.,
67 Stampfli et al., 2002). Nowadays, the Calabrian subduction zone keeps moving south but
68 at a much slower rate, suggesting that the whole system is subjected to opposing forces
69 and/or that its driving mechanism, slab roll-back, is losing efficiency.

70

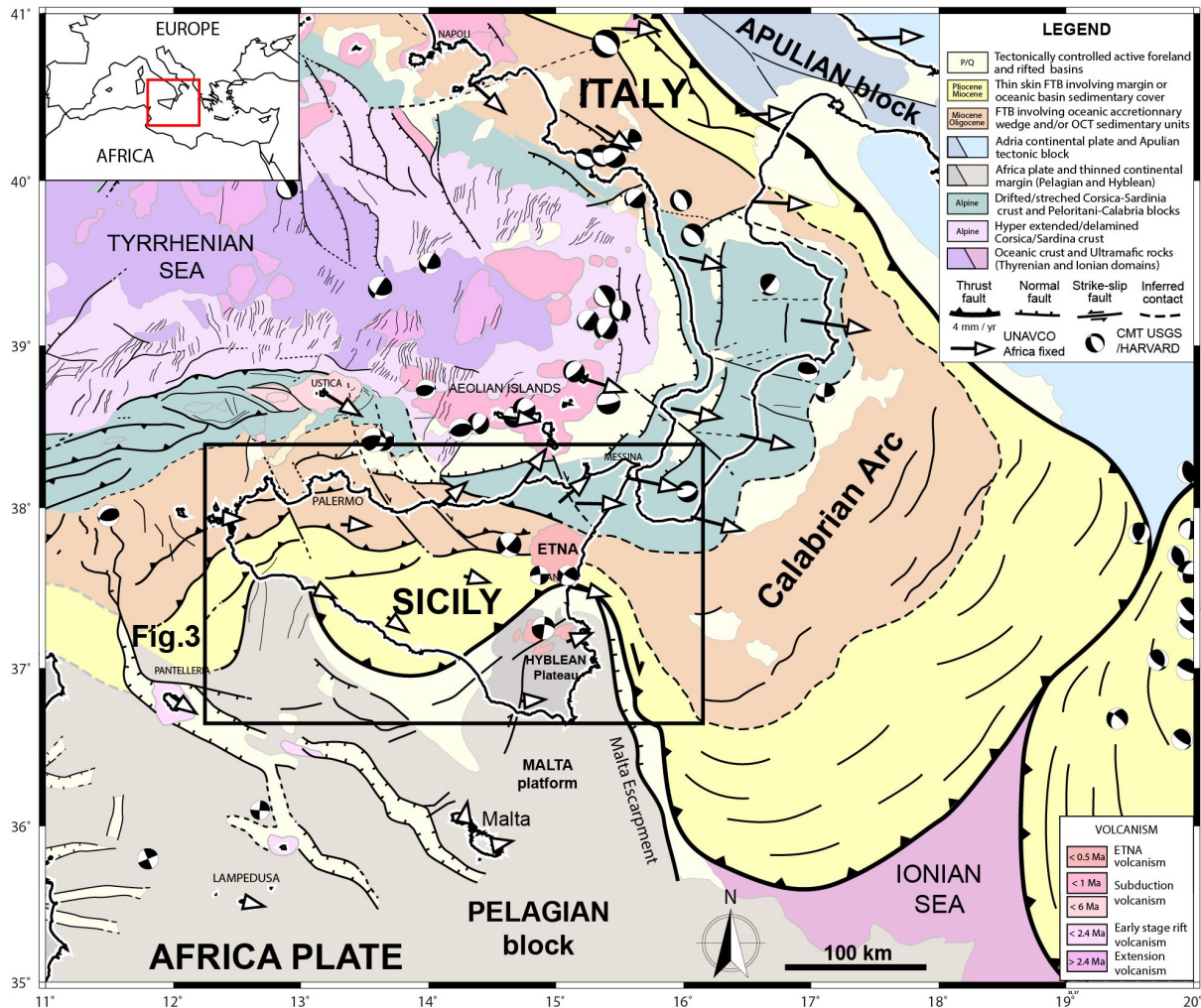


Figure 1 : Geodynamic and tectonic map of Central Mediterranean (modified from Henrquet et al., 2020). Geological and structural data were synthesized from previous publications (e.g., Funicello et al., 1981; Bigi et al., 1991; APAT, 2005; Finetti et al., 2005; Lentini and Carbone, 2014; Prada et al., 2014). Present-day Centroid Moment Tensors ($M_w > 4.5$) and GNSS data were retrieved from <https://www.globalcmt.org/CMTsearch.html> and <https://www.unavco.org/data/gps-gnss/gps-gnss.html> websites, respectively.

71 Recent PS-InSAR satellite measurements (radar interferometry), published by Hen-
 72 riquet et al. (2022), have revealed an unexpected pattern of surface deformation across
 73 Southeastern Sicily, particularly, an eastward increasing subsidence of the whole Hyblean
 74 Plateau (Figure 2). This region has been partially investigated in previous studies, using
 75 similar techniques, but only captured local surface deformation features (Canova et al.,
 76 2012; Vollrath et al., 2017). Up to now, the origin of such a pattern of deformation re-
 77 mains, then, unexplained. Since satellite measurements were acquired over a very short
 78 period compared to typical seismic cycle durations (five versus several hundreds of years),
 79 and considering the discrepancy between satellite measurements and inferred long-term
 80 coastal uplift estimations (e.g., Bianca et al., 1999; Ferranti et al., 2006, 2010; Scicch-
 81 itano et al., 2008; Meschis et al., 2020) (Figure 2a), we hypothesize that the satellite data

82 are representative of the interseismic period. We further infer that the PS-InSAR data
83 mainly document elastic loading mechanisms and reversible deformations. To explain
84 the geodetic observations, we investigate the surface deformation signature of crustal and
85 lithospheric deformation processes, including the impact of the southward migration of
86 the Calabrian subduction system on the structural evolution of the eastern Hyblean mar-
87 gin as well as elastic loading and aseismic creep on coastal and offshore normal faults. We
88 also test the potential surface expression of other processes, such as volcanic deflation,
89 hydrologic loading, and upwelling mantle flow.

90 2 Present-day deformation of SE Sicily

91 The kinematics and active tectonics in ~~the~~ SE Sicily are still a matter of debate, with
92 major evolutions in the last decade (e.g., Bianca et al., 1999; Argnani et al., 2012), in par-
93 ticular with the acquisition of high-resolution bathymetry and seismic **reflection/refraction**
94 profiles in the adjacent Ionian domain (**Argnani and Bonazzi, 2005; Gutscher et al., 2016;**
95 **Dellong et al., 2020**), and **seismotectonic analysis** (e.g., **Gambino et al., 2021, 2022b**).
96 **The** main reasons include the complex polyphased geological history of this region and
97 the relatively low present-day horizontal strain rate (< 5 mm/yr), resulting from **the cul-**
98 **mination of the Calabrian Arc and African Margin collision, and the subsequent** slowdown
99 of the Calabrian subduction (**roll-back and back-arc extension**) ~~zone activity~~ in the last
100 million years (**Goes et al., 2004; D’Agostino et al., 2011; Zitellini et al., 2020**).

101 2.1 Geodesy

102 Geodetic surface measurements in SE Sicily include GNSS (e.g., Palano et al.,
103 2012), PS-InSAR/DInSAR (e.g., Vollrath et al., 2017), and leveling datasets (e.g.,
104 Spampinato et al., 2013).

105

106 PS-InSAR

107 In the present study, we use the first geodetic velocity field covering the whole
108 Island of Sicily published by Henriquet et al. (2022) and derived from Sentinel-1 radar
109 satellite (InSAR data) acquired during the 2015-2020 period. The PS-InSAR pseudo-3D
110 velocity field (Up and E-W component) was obtained by merging ascending and

111 descending acquisitions, combined with a reanalysis of the GNSS time series. Due to the
 112 acquisition geometry, the Sentinel-1 radar satellite is not sensitive to the N-S component
 113 of horizontal surface deformation, which is, fortunately, very low in the studied region
 114 (Henriquet et al., 2022). We therefore consider that, even if affected by minor distortions,
 115 the Up and E-W components of the pseudo-3D velocity data can be used with confidence
 116 (Supplementary Figures S2 to S5). The vertical (Up) component of this dataset reveals
 117 that the central and eastern parts of the Hyblean Plateau experience subsiding rates
 118 increasing eastward from 1 to nearly 3 mm/yr relative to the western coast (Figure 2 and
 119 Supplementary Figure S1). It should be noted that PS-InSAR data also show a slowly
 120 decreasing E-W component to the east of the Hyblean Plateau, with velocities evolving
 121 from 3 to 2 mm/yr (fig.10, Henriquet et al., 2022).

122

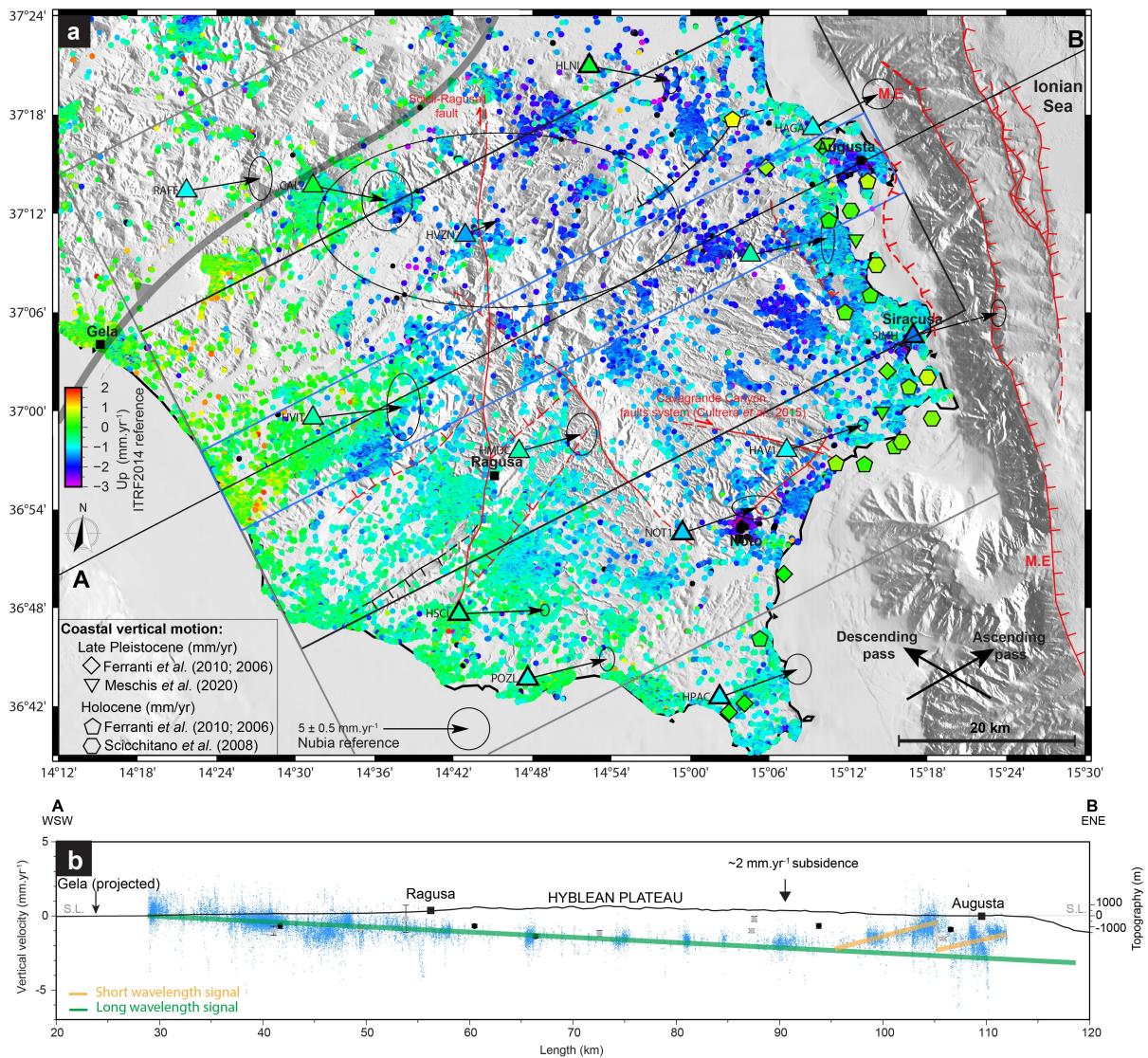


Figure 2 : Geodetic data across the Hyblean Plateau region (see location in Figure 3). *a) The Permanent-Scatterer (PS-InSAR 2015-2020) pseudo-3D Up velocities in map view from Henriquet et al. (2022) and are measured during the 2015-2020 period. GNSS 3D surface velocities are derived from a reanalysis of the Nevada Geodetic Laboratory (NGL) data (Horizontal components reference: fixed Nubia; Up components reference: ITRF2014). Major faults of the Hyblean Plateau (H.P) and Malta Escarpment (M.E) including the offshore normal faults identified by Bianca et al. (1999); Argnani and Bonazzi (2005) and recently analyzed by Gambino et al. (2021) (red: active fault; red dashed: inferred active fault; black: inferred aseismic slip from Spampinato et al. (2013)). b) SW-NE trending velocity profile showing surface velocity (Up) derived from PS-InSAR and GNSS stations vertical velocities. We observed a long wavelength signal (in green) and a short wavelength signal at the eastern part of the H.P (in orange) along the AB profile, and a similar surface deformation is observed to the South of the AB profile (Supplementary Figure S1). PS-InSAR data are stacked across a 5 km width on both sides of the AB profile (in blue). GNSS data are stacked using 20 km (in black) and 40 km (in gray) widths on both sides of the AB profile. Topographic and bathymetric profiles are presented without vertical exaggeration (V.E.x1).*

123 One should note that the zero reference of the PS-InSAR vertical velocity field is
 124 not precisely known. The vertical component of the pseudo-3D PS-InSAR velocity field
 125 and GNSS data have a ± 0.5 mm/yr uncertainty in the ITRF2014 (Altamimi et al., 2016),
 126 which implies that the observed subsidence over the Hyblean Plateau could be a little bit
 127 higher or slower. In the last case, slow uplift rates could be present in the Gela region. The
 128 vertical velocity trend is obtained by projecting and stacking the PS-InSAR data across
 129 a 5 km wide band along an N30°E AB profile (Figure 2b). Along this profile, oriented
 130 perpendicular to the main regional faults, the subsidence velocity reaches, on average, ~ 1
 131 mm/yr between Gela and Ragusa and increases progressively to ~ 2.5 mm/yr between
 132 Ragusa and Augusta. All along the eastern coast, a significantly slower subsidence (or
 133 a relative uplift) is observed. From Augusta to Siracusa, and in the southernmost part
 134 of the Hyblean Plateau (HP), the subsidence rate decreases to about 1 mm/yr compared
 135 to the maximum subsidence rate in the central Hyblean Plateau (Figure 2). In the Gela
 136 region, PS-InSAR vertical velocities indicate a possible slow uplift rate of ~ 0.5 mm/yr
 137 (Figure 2). To the South of the AB profile, a similar surface deformation pattern is
 138 observed; an eastward increase in subsidence rates evolving towards a similar relative
 139 uplift in the coastal (Siracusa) region (Supplementary Figure S1). ~~A second profile, lo-~~
 140 ~~cated 20 km south of the AB profile, shows the same eastward increase of the subsidence~~
 141 ~~rates, evolving towards a similar relative uplift in the Siracusa region (Supplementary~~
 142 ~~Figure S1).~~

143 Along the AB velocity profile, neither the Scicli-Ragusa inferred active fault (Voll-
 144 rath et al., 2017), nor the other major faults of the Hyblean Plateau can be evidenced

145 in **both** the E-W and vertical components of the PS-InSAR data (Henriquet et al., 2022)
146 (Figure 2a), indicating that these faults are locked or are creeping at a slip rate lower
147 than the PS-InSAR resolution (± 0.5 mm/yr). Locally, fast ($\gg 3$ mm/yr) subsiding zones,
148 most probably related to human activities such as water pumping (Canova et al., 2012),
149 can be identified near the main cities of Augusta, Siracusa, and Noto (Figure 2a).

150 Surface deformation signals extending over a hundred or more kilometers are
151 most probably related to crustal or lithospheric scale processes (e.g., Stephenson et al.,
152 2022), whereas those extending over tens of kilometers are likely associated with
153 much shallower and localized mechanical processes such as seismic cycle deformation,
154 volcanic bulging/collapse, hillslope instabilities (landslides), or human activities (water
155 pumping, mining) (e.g., Vilaro et al., 2009). We therefore hypothesize that the
156 PS-InSAR vertical velocity field consists of two superimposed signals: (1) a long
157 wavelength (> 100 km) subsidence, and gradual eastward tilt of the Hyblean Plateau
158 (green line in Figure 2b), compatible with the decreasing PS-InSAR E-W velocities,
159 and (2) a short wavelength signal, extending along the Eastern coast and characterized
160 by sharp variations of the vertical velocities at kilometric scale (orange lines in Figure 2b).

161

162 GNSS

163 The Global Navigation Satellite System (GNSS) data used to calibrate the pseudo-
164 3D PS-InSAR velocity field (Henriquet et al., 2022) were based on the analysis of time
165 series, retrieved from the Nevada Geodetic Laboratory (Blewitt et al., 2018). We refine
166 this analysis by correcting for annual and semiannual seasonal signals, instantaneous
167 offsets, and gaps, using the time series inversion software developed by Masson et al.
168 (2019). Across the Hyblean Plateau, GNSS velocities show horizontal velocities of ~ 2
169 mm/yr oriented homogeneously toward the ENE, in the Nubia reference frame (Figure
170 2). The vertical component of most of the GNSS stations shows an overall subsidence
171 of the HP (-0.8 mm/yr **on** average) in the ITRF2014 reference frame (Altamimi et al.,
172 2016). This tendency is well illustrated by the high-quality NOT1 GNSS station located
173 near the city of Noto, which has recorded the longest time series (23 years, 2000-2023),
174 or by the SSYX and HMDC stations (Supplementary Figures S2 and S3). Overall, the
175 GNSS vertical velocities are consistent with the median of the PS-InSAR vertical velocities
176 calculated over a 3×3 km² region centered on each GNSS station (Supplementary Figures

177 S2 to S5).

178 To estimate the regional horizontal strain rate tensor, we processed the GNSS
179 dataset using the inversion model of Mazzotti et al. (2005). The Hyblean Plateau is
180 characterized by an extension rate oriented $N55^{\circ}E \pm 1^{\circ}$ (close to the AB profile direction)
181 and a shortening rate oriented $N145^{\circ}E \pm 1^{\circ}$ (Supplementary Figure S6), consistent with
182 the focal mechanisms inversion (Figure 3).

183 2.2 Seismology

184 The instrumental seismicity map of SE Sicily, derived from INGV and Rovida et al.
185 (2022) datasets (Figure 3), shows minor to moderate events ($M < 5$) with deep crustal
186 hypocenters (15-30 km). Over the Hyblean Plateau, earthquake hypocenters tend to
187 roughly align along the inferred active, N-S trending, Scicli-Ragusa strike-slip fault (e.g.,
188 Vollrath et al., 2017) and near the Cavagrande Canyon faults system (Cultrera et al., 2015)
189 (Figure 3). Most of these faults are probably inherited from the Plio-Quaternary tectono-
190 magmatic phase of deformation (Henriquet et al., 2019) and were partly re-activated in
191 response to the ongoing Africa-Nubia/Eurasia plates convergence (e.g., Mattia et al., 2012;
192 Cultrera et al., 2015). In this framework, the identification of the seismogenic source that
193 triggered the 1693 event remains debated (e.g., Argnani and Bonazzi, 2005; Bianca et al.,
194 1999). The isoseists of the $M_w \sim 7.4$ Noto earthquake appear largely open toward the
195 Malta Escarpment and Ionian Sea domains, suggesting the seismogenic fault is located
196 offshore (Figure 3). East of the Hyblean Plateau, earthquakes essentially distribute along
197 the Malta Escarpment where a normal fault system, potentially responsible for the 1693
198 earthquake, has been identified (e.g., Bianca et al., 1999; Argnani and Bonazzi, 2005;
199 Gambino et al., 2021, 2022b), (Figure 3).

200 The focal mechanisms over the Hyblean Plateau have dominant strike-slip charac-
201 teristics, contrasting with the extensional deformation characterizing the NE corner of
202 Sicily (Figure 3).

203

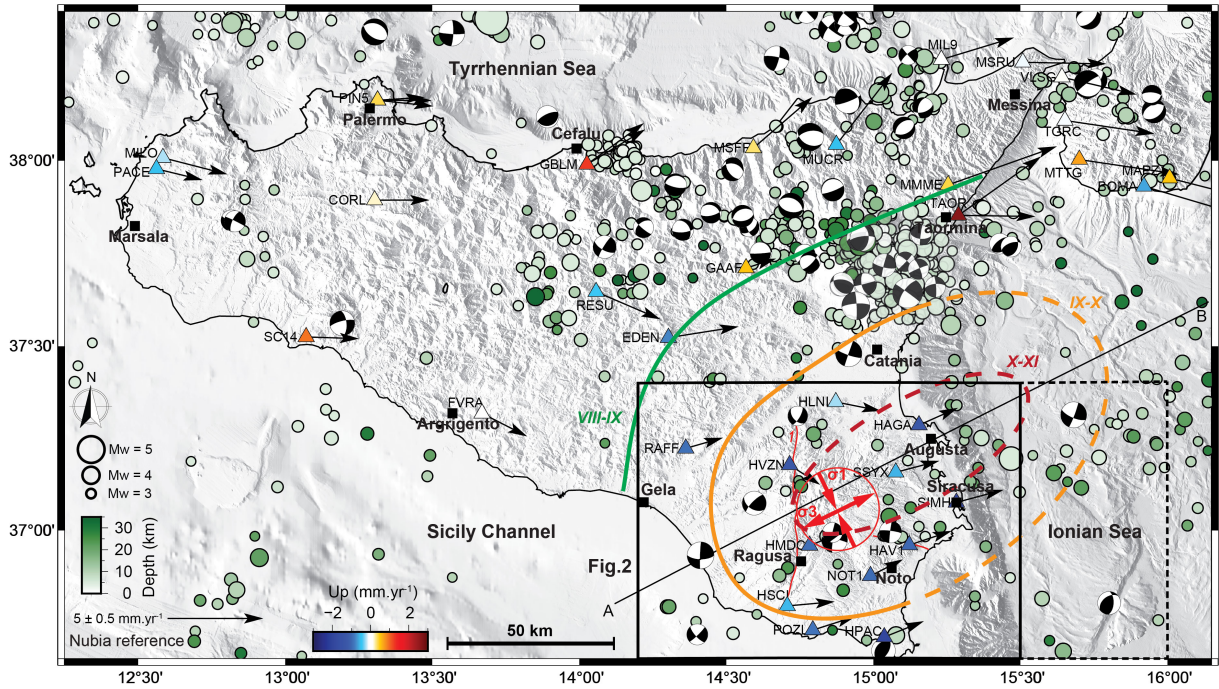


Figure 3 : Instrumental seismicity of Sicily at crustal scale (0-30 km depth) showing earthquake hypocentral locations and focal mechanism solutions of $M > 3$ events from 1985 to 2022 Istituto Nazionale di Geofisica e Vulcanologia (INGV) (2005); Scognamiglio et al. (2006). 3D surface velocity derived from GNSS time series published in Henriquet et al. (2022) (Horizontal components reference: fixed Nubia; Up components reference: ITRF2014). Macroseismic intensity data of the 1693 Val-di-Noto Earthquake ($M \sim 7.4$) from INGV CPTI15 database (Rovida et al., 2022): red dashed line = X-XI intensity, orange dashed line = IX-X intensity, green dashed line = VIII-IX intensity). Focal mechanisms stress inversion (red arrows) for the Hyblean Plateau region (black frame) and Ionian Sea (black dashed frame) using Michael's method (Vavryčuk, 2014; Levandowski et al., 2018). The AB profile shows the location of the PS-InSAR profile and synthetic structural cross-section presented in Figures 2 and 4.

204 To estimate the present-day regional stress field across SE Sicily, we analyzed
 205 the available focal mechanisms using the Vavryčuk's numerical model (Vavryčuk, 2014;
 206 Levandowski et al., 2018), based on Michael's method (Michael, 1984). Results show that
 207 the regional stress across SE Sicily (Figure 3) is homogeneous (Supplementary Figures S7
 208 and S8). The maximum compressive stress (σ_1) is horizontal and oriented $N154^\circ E \pm 7^\circ$,
 209 compatible with the $N160^\circ E$ Africa-Eurasia plates convergence (e.g., Mattia et al., 2012;
 210 Kreemer et al., 2014). The minimum stress (σ_3) is oriented $N64^\circ E \pm 7^\circ$, compatible with
 211 the extension rate derived from GNSS data inversion (Figure 3).

212 If this regional stress field is compatible with the measured geodetic PS-InSAR
 213 surface deformation data (E-W bending generating extensional stress), it does not explain
 214 the observed eastward-increasing subsidence rate across the HP.

215 2.3 Synthetic structural profile

216 To **better** constrain the deep structure and rheology of the studied area, we synthe-
217 size the available geological and geophysical data into a 200 km long simplified crustal-scale
218 structural cross-section following the N30°E AB profile. **This section incorporates part**
219 **of** the Hyblean Platform, the Malta Escarpment, the western Ionian domain, **and cut,**
220 **almost perpendicularly,** the offshore normal faults **along the Malta Escarpment and the**
221 **Alfeo/Ionian strike-slip fault systems, extending eastward** (Figures 2, 3 and 4). The east-
222 ern part of the synthetic structural profile is mainly based on seismic refraction profiles
223 from [Dellong et al. \(2018, 2020\)](#), particularly the DY-P3 profile running sub-parallel to
224 the AB profile and located 20 km further North, as well as seismic reflection profiles from
225 [Argnani et al. \(2012\)](#); [Gutscher et al. \(2016\)](#); [Tugend et al. \(2019\)](#); [Gambino et al. \(2021,](#)
226 [2022b\)](#) (Figure 4c). The structure of the western section is constrained by onshore and
227 **offshore** geology, well log stratigraphy, geophysics, seismic reflection profiles, and geologi-
228 cal cross-sections from the ViDEPI project, [Lentini and Carbone \(2014\)](#), [Lipparini et al.](#)
229 [\(2023\)](#), [Scarfi et al. \(2018\)](#), [Henriquet et al. \(2019\)](#) and [Finetti et al. \(2005\)](#).

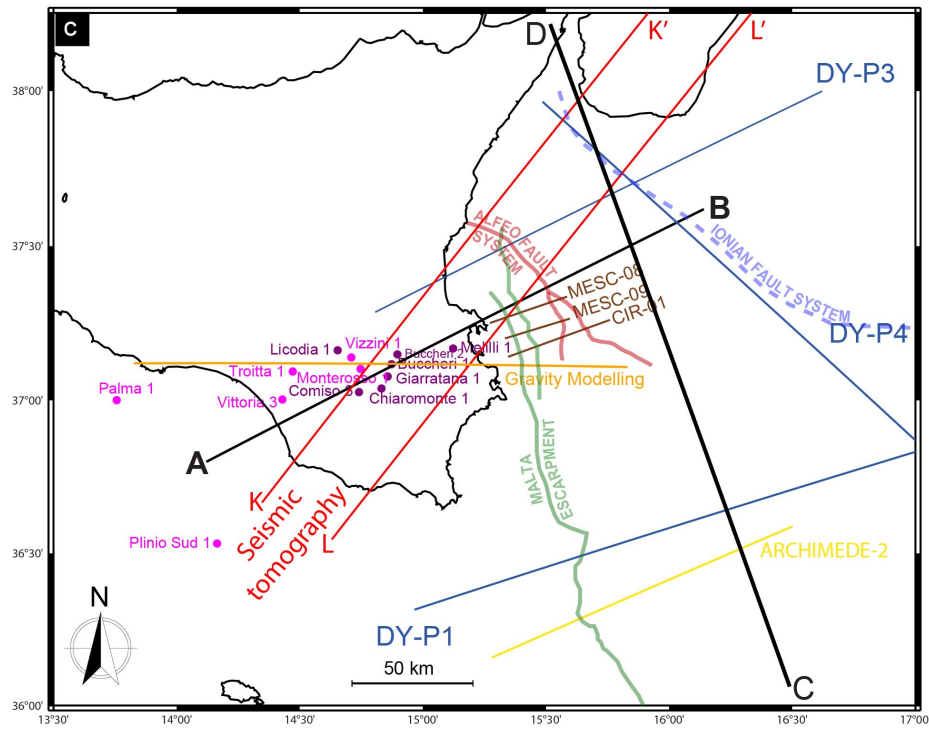
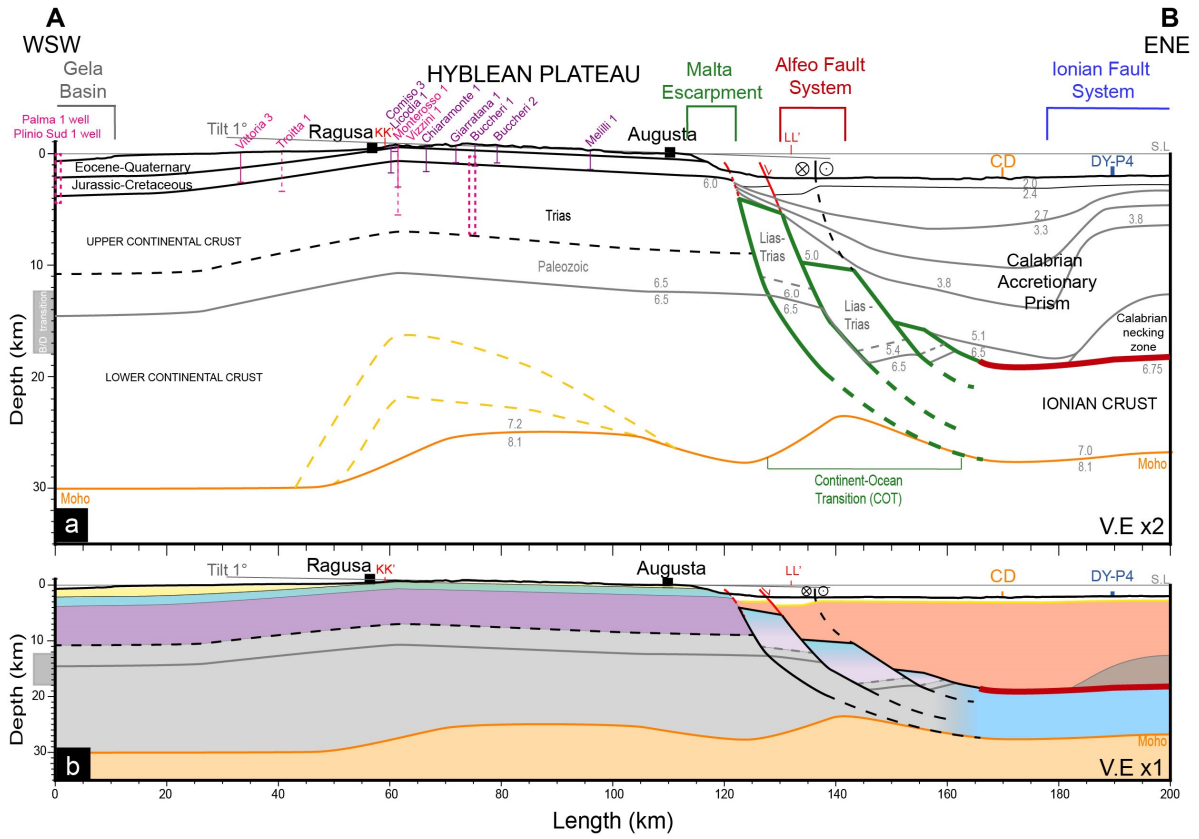


Figure 4 : Simplified crustal cross-section along the $N30^{\circ}E$ AB profile (see Figures 4c and 2 for location). a) Two times vertically exaggerated synthetic structural profile along with seismic velocity data showing the structure and rheology of the Hyblean Plateau and eastern oceanic domain determined from onshore and offshore geology, wells stratigraphy, geophysics, seismic reflection, and refraction profiles (see [Supplementary Figure S9](#) for references). Note the 1° tilt of the Hyblean Plateau topography toward the East. The red line corresponds to the inferred position of the main subduction décollement, and the green lines, refer to our interpretation of tilted blocks from the Malta Escarpment (M.E). b) The synthetic structural profile shows the potential geological layers and structural deduced by, essentially, wells data for onshore domain and seismic refraction for offshore domain profiles, respectively, without vertical exaggeration (V.E.x1). c) Locations, in map view, of the AB profile, [ViDEPI project](#) wells data, tomography profile, refraction, and reflection seismic profiles.

230 In the Hyblean domain, geophysical data (e.g., SgROI et al., 2012; Milano et al., 2020)
 231 indicate that the crust has an average thickness of ~ 30 -35 km, with a notable difference
 232 in the Hyblean Plateau region, marked by a huge positive Bouguer anomaly. Based on
 233 gravity data modeling, Henriquet et al. (2019) showed that this gravity anomaly can be
 234 explained by a 100 km-large high-density lower crustal body, compatible with a local
 235 Moho uplift to a depth of about 20-25 km. This last interpretation seems also supported
 236 by recent tomographic data (Scarfi et al., 2018). We constrain the geometries of the
 237 Quaternary to Mesozoic sedimentary units of the Hyblean Platform and Gela basin are
 238 constrain using the Monterosso 1, Plinio Sud 1, Troitta 1, Vittoria 3, Vizzini 1 wells from
 239 ViDEPI project (in pink, Figure 4c and Supplementary Figure S9), the Chiaramonte 1 and
 240 Mellili 1 wells from Lentini and Carbone (2014), and Buccheri 1-2, Comiso 3, Giarratana
 241 1 and Licodia 1 wells from Lipparini et al. (2023) (in purple, Figure 4c and Supplementary
 242 Figure S9). We also used the top of the Upper Triassic (Gela formation) isobaths published
 243 by Lipparini et al. (2023)

244 In the DY-P3 seismic refraction profile (Dellong et al., 2018), the 6.0 and 6.5 km/s
 245 velocity contours delimit two main steps deepening eastward at the junction between
 246 the Hyblean continental and Ionian oceanic domains (Figures 4a and 4b). Considering
 247 their locations along the Malta Escarpment that outlines the Continent-Ocean Transition
 248 (COT), we interpret these velocity variations as deepening of the sediment/basement
 249 boundary, potentially related to tilted blocks of thinned continental crust formed during
 250 the Permo-Triassic/Early Jurassic rifting phase (see section 1) (e.g., Scandone et al., 1981;
 251 Minelli and Faccenna, 2010; Dellong et al., 2018; Tugend et al., 2019). Our interpretation
 252 of tilted blocks at the continent-ocean transition is consistent with similar considerations
 253 analyzing seismic reflection/refraction profiles (e.g., Afilhado et al., 2015; Sapin et al.,

254 2021; Klingelhofer et al., 2022).

255 As documented in Argnani and Bonazzi (2005), Gutscher et al. (2016), and Gambino
256 et al. (2021, 2022b), the seismic reflection profiles (MESC-O6, MESC-11, CIR-01, MESC-
257 08, and MESC-09) show several normal faults bounding and crossing the Turbiditic Valley,
258 extending along the base of the Malta Escarpment (Gutscher et al., 2016). The Turbiditic
259 Valley fault system is constituted by three ~~major~~ parallel normal faults, ~ 60 km long,
260 producing a marked morphological offset of the Ionian seafloor from the latitudes of
261 Catania to Siracusa (Figures 4a and 4b). These faults dip $35-50^\circ$ to the East and most
262 probably merge at depth into a single major fault plane (Argnani and Bonazzi 2005;
263 Argnani 2021; cf. MESC-08 and MESC-09 seismic reflection profiles in Gambino et al.
264 2021). These offshore normal faults could be linked to the recent re-activation of crustal
265 faults at the Ocean-Continent Transition, inherited from the Early Mesozoic rifting phase
266 (Figures 4a and 4b).

267 On the eastern side of the Hyblean domain, the Moho is constrained by DY-P3
268 and DY-P1 refraction profiles to a depth of ~ 30 km below the Malta Escarpment. To the
269 east, in response to the bending of the Ionian slab, the Moho deepens northward from 20
270 km (DY-P1) to 32 km (DY-P3). Based on these data and the DY-P4 refraction profile
271 (Dellong et al., 2020), we estimate the depth of the Moho below the Ionian oceanic crust
272 to be about 25-30 km in the eastern part of the AB synthetic profile. In this region, the
273 domain delimited by the seismic refraction velocities of 3.8-5.1 km/s has been interpreted
274 as corresponding to the deformed sediments of the Calabrian accretionary prism (CAP)
275 (Dellong et al., 2018). Its thickness increases from 5 km (DY-P1) to 15 km (DY-P3), and
276 it is evaluated to be ~ 15 km along the AB profile (Figures 4a and 4b). Note that a portion
277 of the southern termination of the Calabrian Arc (i.e., Hercynian basement) is probably
278 present in the AB profile according to the seismic refraction DY-P4 profiles (Dellong et al.,
279 2020) (Figures 4a and 4b). The location of the main subduction décollement along the
280 AB profile has been estimated at a depth of ~ 20 km (thick red line in Figure 4a) using
281 the sharp velocity step of 6.75 km/s (5.1-6.1 km/s) seismic refraction DY-P3 and DY-P4
282 profiles (Dellong et al., 2018).

3 Mechanical model hypotheses

To explain the long wavelength bending trend evidenced by the PS-InSAR Up component, we model the flexure of the Hyblean Plateau induced by (1) overloading of the continent-ocean transition (COT) domain in response to the SE migration of the very thick Calabrian accretionary prism (CAP), and (2) forced subsidence of the COT due to the local increase of the slab pull force imposed by the southward roll-back of the Ionian subduction. We hypothesize that these crustal/lithospheric deformation mechanisms may be strong enough to bend the adjacent Hyblean domain and induce the large-scale subsidence and tilt evidenced by the geodetic data (PS-InSAR and GNSS) (Figure 2b). In addition, we test interseismic loading models on several onshore and offshore east-dipping normal faults, such as the Augusta-Siracusa fault, the Malta Escarpment, and the active faults documented by Bianca et al. (1999); Argnani and Bonazzi (2005), Gutscher et al. (2016) and Gambino et al. (2021, 2022b), to explain the short wavelength deformation signal (relative uplift) extending along the eastern coast of the Hyblean Plateau (Figure 2b).

3.1 Lithospheric flexure along a NNW-SSE profile

To better constrain key flexural parameters, such as the rigidity of the Hyblean and Ionian crust/lithospheres, the slab-pull force, and to investigate the impact of the Ionian slab roll-back, we first model the bending of the subducting Ionian slab along a NNW-SSE profile (CD profile), trending orthogonal to the AB profile (Figure 5a). We compare the Ionian slab geometries with Hayes et al. (2018) and Maesano et al. (2017) datasets with the depth of the top oceanic crust from Dellong et al. (2018) seismic refraction data (Supplementary Figure S10). In the southern part of the CD profile, the Maesano et al. (2017) dataset indicates shallower depths (~5 km), compared to Hayes et al. (2018) and Dellong et al. (2018, 2020) data, because the main décollement jumps away from the top of the Ionian oceanic crust to a higher level in the sedimentary cover (Supplementary Figure S10). Note that in the northern part of the CD profile, the Maesano et al. (2017) dataset indicates also shallower depth compare to Hayes et al. (2018) dataset.

Finally, we decided to use, as a structural reference, the isobaths of the top of the Ionian slab published by Hayes et al. (2018), because it correlates with the top of the

313 oceanic crust depths derived from the seismic refraction data (Dellong et al., 2018, 2020)
314 (Figure 5a)..

315 The lithosphere flexure models (as well as those in section 3.2) are calculated
316 using the gFlex software (Wickert, 2016). We impose a no-displacement condition at the
317 southern profile boundary and a broken plate with no bending moment and no shear at
318 the northern boundary. The Ionian oceanic lithosphere is modeled assuming an effective
319 elastic thickness (T_e) ranging from 25 to 37 km (Figure 5b and Supplementary Figure S11)
320 compatible with its Triassic to early Jurassic age (e.g., Catalano et al., 2001; Speranza
321 et al., 2012) and consistent with other publications (e.g., Watts and Zhong, 2000; Tesauero
322 et al., 2012; Cloetingh et al., 2015).

323 The flexure of the subducting slab depends on its mechanical properties and the
324 loads induced by the sedimentary cover, the accretionary prism, and the slab pull force
325 (Figure 5b). According to seismic refraction profiles DY-P1 and DY-P4 (Dellong et al.,
326 2018, 2020), the undeformed ante-Messinian sedimentary cover overlying the Ionian crust
327 has a thickness of about 5 km. Thus, taking into account a depth of the Ionian Sea of
328 5-6 km, we consider that the top of the Ionian crust was lying at a uniform depth of
329 10-11 km before the onset of the Calabrian subduction system (Figure 5b). This depth
330 corresponds to the isostatic equilibrium for the Ionian crust. It determines the initial
331 geometry of the flexural model from which we calculate the bending induced by the
332 Calabrian accretionary prism (CAP) load.

333

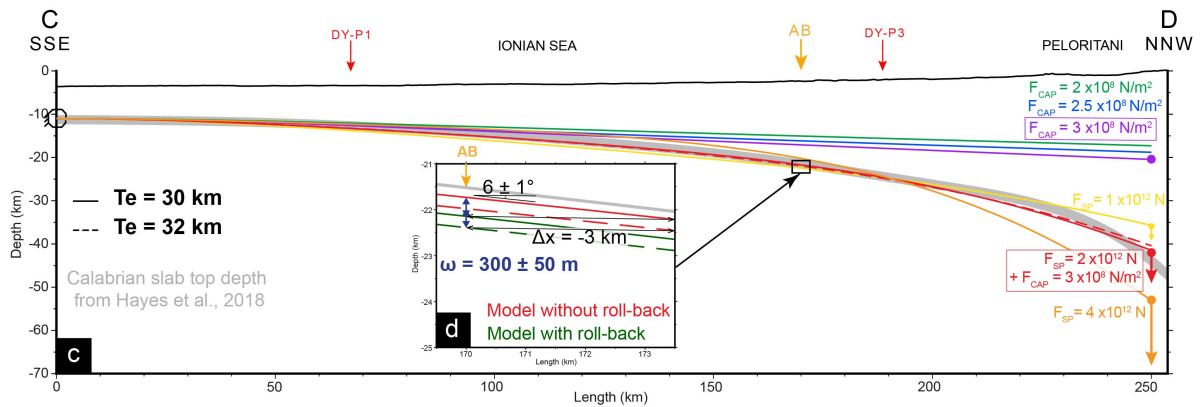
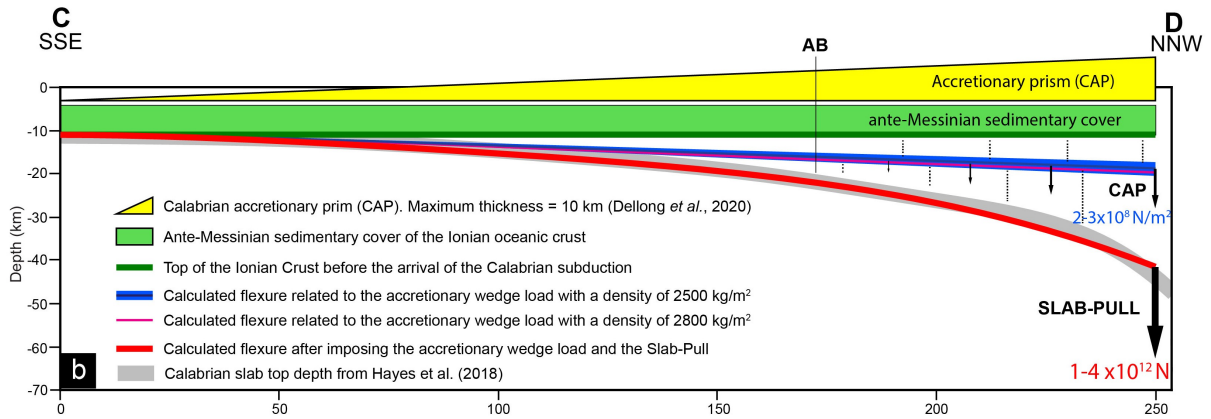
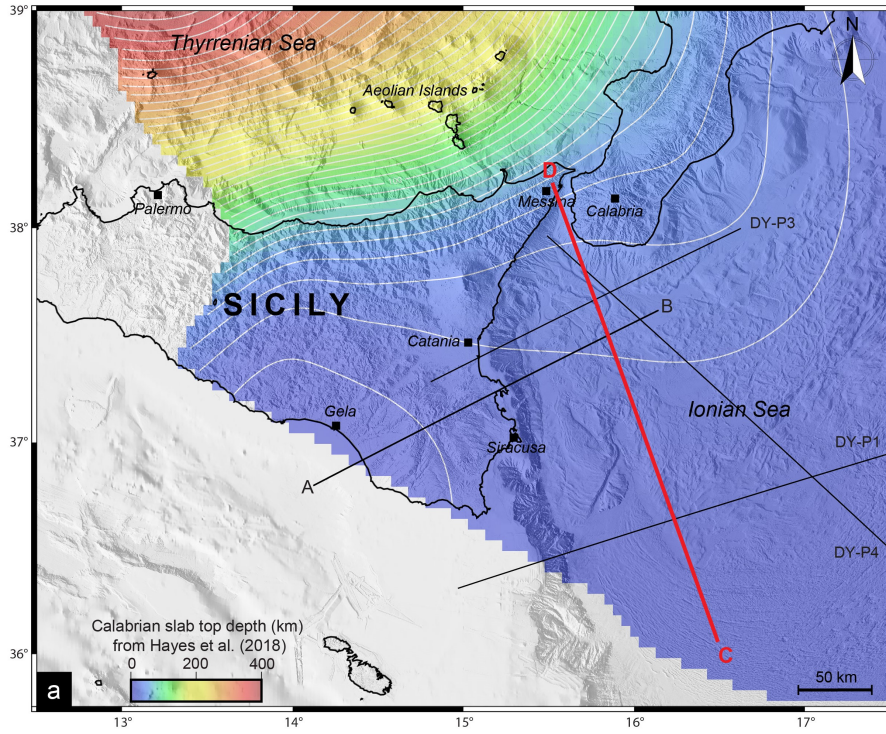


Figure 5 : a) Map and isobaths of the top of the Ionian slab subducting below the Calabrian Arc (Hayes et al., 2018) with seismic refraction profiles from Dellong et al. (2018, 2020), also used to constrain the top of the Ionian oceanic crust. b) NNW-SSE trending CD cross-section (in gray) showing the flat and ramp geometry of the Ionian slab (see location in Figure 5a). The Ionian oceanic lithosphere supports a 5 km thick homogeneous Paleogene sedimentary cover (in green). The CAP (in yellow) thickness increases northward up to ~ 15 km (Dellong et al., 2020). The associated flexure (in blue) is calculated with density ranging from 2500 kg/m^2 to 2800 kg/m^2 (in darkblue and pink). The bending of the slab is controlled by the slab pull, represented as a punctual load, ranging from $1-4 \times 10^{12}$ N (in red). c) The Paleogene cover and the CAP load are performed with a maximum CAP load of $2 \times 10^8 - 3 \times 10^8 \text{ N/m}^2$. Flexural models are performed with effective elastic thicknesses (T_e) ranging from 25 to 37 km and slab pull forces ranging from 1×10^{12} to 4×10^{12} N (Supplementary Figure S11). Topographic, slab, and flexural model profiles are presented without vertical exaggeration (V.E.x1). d) Zoom of profiles CD and AB intersection showing the depth difference between favorite models: CAP load of $3 \times 10^8 \text{ N/m}^2$, slab pull of 2×10^{12} N, elastic thickness of 30 (continuous line) and 32 (dashed line) km, without rollback (red line) and with rollback (green line). The local subsidence associated with the 3 km/Myr slab SE retreat is estimated to be about 300 ± 50 m.

334 Based on seismic refraction profiles DY-P4, DY-P1, and DY-P3 (Dellong et al., 2018,
 335 2020), the Calabrian accretionary prism thickness increases northward from 5 to 15 km.
 336 By removing the initial 5 km-thick Ionian sedimentary cover, the CAP load represents
 337 an increase in sediment thickness from 0 km at the southern end of the CD profile to 10
 338 km at the northern end. The Calabrian backstop, made of Hercynian continental crust,
 339 is not taken into account (Figure 5b).

340 The CAP load is calculated by:

$$F_{CAP} = \rho gh \quad (1)$$

341 with a sediment density (ρ) of $2500-2800 \text{ kg/m}^2$ (profile 2D) using to Dellong et al. (2020),
 342 a gravity acceleration (g) of 9.81 m/s^2 , and an increase of the CAP thicknesses (h) from 0
 343 to 10 km. We also calculated the CAP load using an end-member density of 2800 kg/m^2
 344 (Figure 5b), which resulted in a variation in flexure amplitude of a few percent, thus not
 345 affecting the results of continental flexural models.

346 The CAP load (F_{CAP}) is applied on the CD profile divided into 1-km-long segments
 347 by imposing a northward linear gradient from 0 to $2.45 \times 10^8 \text{ N/m}^2$ (equation 1) on the
 348 first 250 km of the profile (Figures 5b and 5c). We perform several tests with different
 349 maximum CAP load (F_{CAP}) and elastic thicknesses (T_e) ranging from 2×10^8 to $3 \times$
 350 10^8 N/m^2 and 25 to 37 km, respectively. Models are tested with a constant mantle density
 351 of 3300 kg/m^2 and no filling density for mantle restoration force (Figure 5c). The resulting
 352 flexure (~ 8 km maximum), even if significant, is not sufficient to fit the Ionian slab profile

353 (gray line in Figures 5b and 5c).

354 The slab pull force is then added to the northern termination of the Ionian litho-
355 sphere as a point load (Figure 5b). Flexural models are tested with different slab pull
356 forces ranging from 1×10^{12} to 4×10^{12} N, consistent with other publications reviewing
357 slab rollback mechanical properties (e.g., Lallemand et al., 2008) and the same range of
358 elastic thicknesses from 25 to 37 km (Figure 5c and Supplementary Figure S11). The best
359 fit to the Calabrian Ionian slab top profile is obtained for elastic thicknesses (T_e) of 30-32
360 km, a maximum accretionary wedge load (F_{CAP}) of $3 \times 10^8 \text{ N/m}^2$, and a slab pull force
361 (F_{SP}) of 2×10^{12} N (Figure 5c and Supplementary Figure S11). It's worth noting that
362 including the CAP load significantly reduces the amplitude of the forebulge associated
363 with slab bending, resulting in a flat-and-ramp geometry similar to that of the Ionian
364 slab.

365 3.2 Crustal flexure along a WSW-ENE profile

366 The impact of the Ionian subduction roll-back on the deformation of the Hyblean
367 Plateau is evaluated along the N30°E trending AB profile (Figure 5a), considering based
368 on the following simplifications: (1) The ongoing roll-back induces incremental changes
369 in the slab profile that corresponds can be matched with to a southward translation and
370 local deepening of the slab geometry, inducing a local deepening. (2) This results in a
371 local incremental increase of the accretionary prism thickness. (3) Due to the mechan-
372 ical coupling of the Ionian slab and Hyblean lithosphere, the slab deepening exerts an
373 incremental downward force on the COT (Figure 6).

374 The effective elastic thickness of the Hyblean lithosphere is less constrainable than
375 that of the Ionian lithosphere but should remain within standard values for a regular
376 undeformed continental crust with an average geotherm. We test elastic thicknesses (T_e)
377 ranging from 25 to 40 km (Figure 6), assuming a uniform thickness, considering that the
378 continent-ocean transition and the oceanic lithosphere have the same elastic rigidity as
379 the Hyblean crust. Finally, we also considered that none of the fault systems offshore
380 SE Sicily are mature enough to significantly affect the mechanical properties of the
381 above-mentioned crustal/lithospheric blocks (e.g., Gambino et al., 2022a).

382

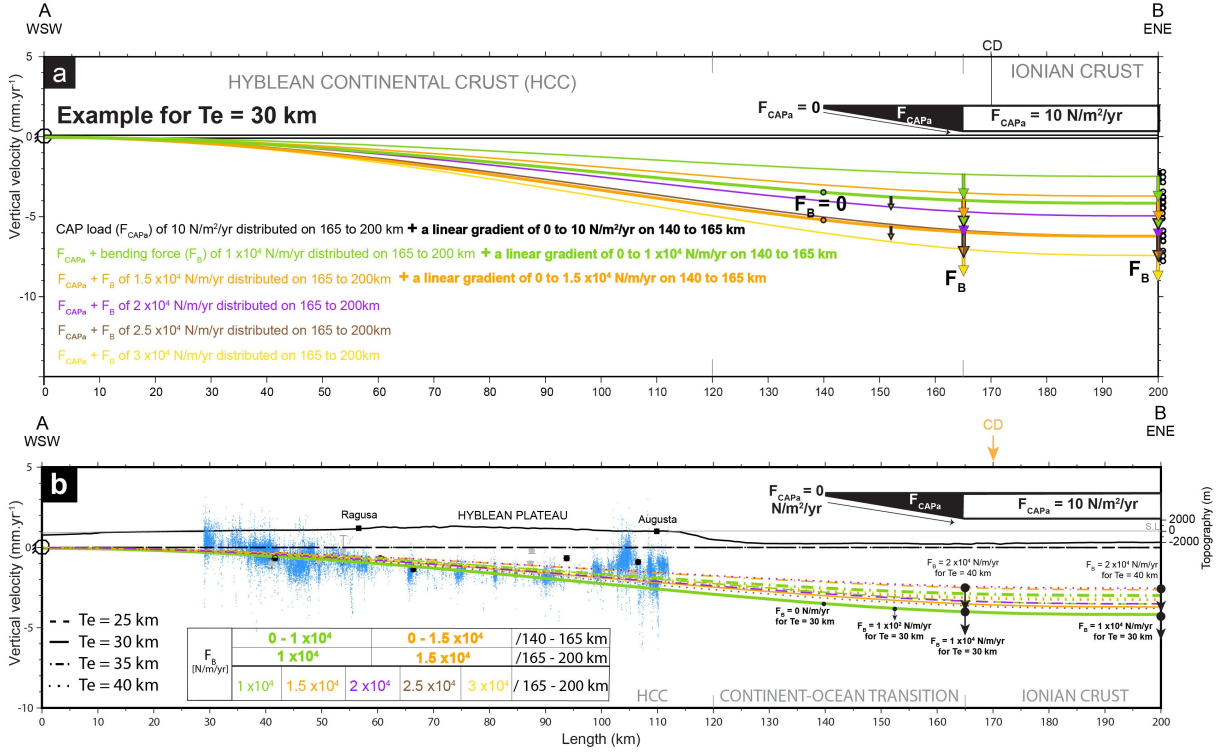


Figure 6 : a) Continental crustal flexure is controlled by the southward retreat of the Ionian slab. We calculated the flexure ($gFlex$ from Wickert, 2016) induced by the only CAP load (F_{CAPa}) of $10 \text{ N/m}^2/\text{yr}$ distributed on the Continent-Ocean Transition (in black), and on the adjacent Ionian crust (in white). For an elastic thickness of 30 km, best models have a bending forces (F_B) of $1 \times 10^4 \text{ N/m/yr}$ (in green), $1.5 \times 10^4 \text{ N/m/yr}$ (in orange), $2 \times 10^4 \text{ N/m/yr}$ (in purple), $2.5 \times 10^4 \text{ N/m/yr}$ (in brown), and $3 \times 10^4 \text{ N/m/yr}$ (in yellow) distributed on the only adjacent Ionian crust or including also part of the COT (see also Supplementary Figure S12). b) Best models (Supplementary Figure S12) are compatible with a wide range of elastic thicknesses (25-40 km). PS-InSAR vertical velocities (in blue) and GNSS vertical velocities with their uncertainties. Topographic and bathymetric profiles are presented without vertical exaggeration ($V.E.x1$).

383 We first evaluate the flexural response due solely to the local incremental increase
384 of the CAP load induced by its southward migration of the slab profile, using our previous
385 analysis of the bending of the Ionian slab. Based on the velocities of the GNSS stations
386 situated in Calabria, we estimate the southward migration to 3 mm/yr , compared to a
387 fixed Hyblean Plateau (Henriquet et al., 2022). At the intersection between AB and CD
388 profiles, at the 170 km length mark in the CD profile, the Ionian slab dips $6 \pm 1^\circ$ toward
389 the north (Hayes et al., 2018) (Figure 5d). Taking into account the CAP geometry, its
390 southward motion, and the slab geometry, we calculate a local incremental thickening of
391 the CAP of $3 \times 10^{-4} \text{ m/yr}$ (equivalent to 300 m/Myr) and a resulting load (F_{CAPa}) of
392 about $5\text{-}10 \text{ N/m}^2/\text{yr}$ (Figure 5d). Applying a linear load gradient starting from zero at
393 the base of the Malta Escarpment (140 km marks of the AB profile) to $5\text{-}10 \text{ N/m}^2/\text{yr}$ at
394 the end of the continent-ocean transition (165 km marks of the AB profile), then applying
395 this constantly load until the end of the AB profile results in a slow onshore subsidence

396 rate of $1.5 \times 10^{-4} \pm 5 \times 10^{-5}$ mm/yr maximum, 20 000 time smaller than the PS-InSAR
 397 subsidence rate measured in the same area (~ 3 mm/yr).

398 We then investigate the effect of the southward Ionian slab roll-back and associ-
 399 ated downward pull on the COT. We first calculate the flexural rigidity of the oceanic
 400 lithosphere (Turcotte and Schubert, 2014):

$$D = \frac{ETe^3}{12(1 - \nu^2)} \quad (2)$$

401 with a Young modulus (E) of 1×10^{11} Pa, a Poisson's ratio (ν) of 0.25, and effective
 402 elastic thicknesses (Te) of 30-32 km (see 3.1). We obtain a flexural rigidity (D) of the
 403 Ionian lithosphere of $2.4\text{-}2.9 \times 10^{23}$ Pa m³.

404

405 To simulate the Ionian slab retreat, we translate the slab profile southward, as-
 406 suming a slab retreat velocity of ~ 3 mm/yr (D'Agostino et al., 2011) (Figure 5d). At
 407 the intersection of profiles AB and CD, this induces an incremental deepening of the Io-
 408 nian slab of about 3×10^{-4} m/yr (equivalent to 300 m/Myr), which defines the equivalent
 409 downward force at the same location along the CD flexure profile (Turcotte and Schubert,
 410 2014):

$$F_B = \frac{\omega 2D}{x^2(L - \frac{x}{3})} \quad (3)$$

411 with an incremental deflection (ω) of 3×10^{-4} m/yr (Figure 5d) and a flexural rigidity
 412 (D) of $2.4\text{-}2.9 \times 10^{23}$ Pa m³. The total profile length L corresponds to the point of the
 413 Hyblean lithosphere where the deflection (ω) is null, ~ 200 km based on the PS-InSAR and
 414 structural data (Figure 6). The distance x corresponds to the point where the deflection
 415 (ω) is estimated (intersection with profile CD). Considering $L = 250 \pm 50$ km and $x =$
 416 150 km, the equivalent incremental downward force is about $1\text{-}6.5 \times 10^4$ N/m/yr.

417 This equivalent force (F_B) is then applied on the AB profile to model, with gFlex,
 418 the resulting flexure of the Hyblean crust/lithosphere. Flexural models are calculated
 419 with a no-displacement boundary condition at the southwestern end of the profile (20 km
 420 west of Gela) and a free displacement of a horizontally clamped boundary condition at
 421 its northeastern end (80 km East of Malta Escarpment). Flexural models are run with
 422 a fill density of 2500 kg/m² (2D profile) solely for the CAP load. The downward force

423 (F_B) and CAP load (F_{CAPa}) are **homogeneously applied as constant loads** (on 1-km-long
424 segments) over the **35 or 60-km** long portion of the AB profile corresponding to the only
425 **adjacent Ionian crustal domain, and from the base of the Malta Escarpment to the end of**
426 **the COT, as a linear load gradient evolving from zero to the maximum calculated load.**
427 We test different elastic thicknesses (T_e) and bending force (F_B) ranging from 25 to 40
428 km and 1×10^4 to 6.5×10^4 N/m/yr, respectively (Figure 6b and Supplementary Figure
429 S12).

430 To determine the best Hyblean crustal flexure models, we first filter the PS-InSAR
431 vertical velocities (5 km stacked of the AB profile) using a 5 km width median filter with
432 a step of 1 km. Comparing the resulting long-wavelength trend of the PS-InSAR data
433 with **all** flexural models shows **maximum** misfits of **about 12 mm/yr**. The comparison
434 **between the** GNSS data (20 km stacked of the AB profile and 5 km large median filter
435 with a step of 1 km) shows a **little bit** higher **maximum** misfit of **about 13 mm/yr** due
436 to a variable spatial density and quality of GNSS stations over the Hyblean Plateau
437 (Supplementary Figure S12c). The best models (**0.5 mm/yr** RMS PS-InSAR) have ~~elas-~~
438 ~~tic thicknesses of 30 to 40 km,~~ a CAP load plus a bending force ranging from 1×10^4 to
439 3×10^4 N/m/yr distributed on a 35 km long portion of the AB profile, and also between
440 1×10^4 to 1.5×10^4 N/m/yr distributed on a 60 km long portion of the AB profile, with
441 **effective elastic thicknesses ranging from 25 to 40 km** (Figure 6b, and Supplementary
442 Figures S12b, S12c). None of the tested continental crustal flexure models reproduce the
443 short wavelength deformations observed in the Gela region (slow uplift of ~ 0.5 mm/yr)
444 or along the Augusta-Siracusa coastal area (**relative uplift of 1-2 mm/yr**).

445 **3.3 Interseismic loading and aseismic creep on coastal and off-** 446 **shore faults**

447 Along the coast, from Augusta to Siracusa, PS-InSAR vertical velocities vary at
448 a kilometer-scale and appear 1-3 mm/yr slower than the general trend of subsidence
449 affecting the Eastern Hyblean Plateau (Figures 2a and 6b). Interestingly, these short
450 wavelength signals show triangular patterns similar to those produced by shallow faulting
451 in an elastic domain. To investigate the sources of these surface deformations, we test
452 several scenarios involving interseismic loading and aseismic creep on coastal and offshore

453 faults.

454 Offshore, several active normal faults, outcropping along the base of the Malta
455 Escarpment, have been identified, imaged and documented in detail by Argnani and
456 Bonazzi (2005); Gutscher et al. (2016); Gambino et al. (2021, 2022b). Close to the coast-
457 line, the offshore Augusta-Siracusa fault (Figure 7) has also been considered as a potential
458 active fault (e.g., Bianca et al., 1999; Azzaro and Barbano, 2000). We use the Coulomb
459 3.4 software (Toda et al., 2011) to impose different fault slip rates and geometric boundary
460 conditions on these fault systems, assuming standard elastic properties (Poisson's ratio of
461 0.25, Young modulus of 80 GPa).

462 The fault plane geometries tested (strike, dip) are based on published field-trip
463 observations and measurements (Gambino et al., 2021). Fault locations are based on
464 published geological/structural maps (Adam et al., 2000) and on the presence of sharp
465 gradients in the PS-InSAR velocity pattern. The imposed fault slip velocities result from
466 a trial-and-error empirical approach. The objective, essentially, is to evaluate if aseismic
467 slip on known and unknown faults could generate sufficient surface deformation to explain
468 the measured surface deformation pattern.

469 The model predictions are compared to the PS-InSAR short wave-length signals
470 (Figure 7b) obtained by removing the mean of best-fitting flexural models (see section
471 3.2) from the original geodetic dataset. Two patterns of relative uplifts of about $2.5 \pm$
472 0.5 mm/yr, gently tapering westward, can be identified near and to the SE of Augusta
473 with a zone of relative subsidence of about -2 ± 1 mm/yr in between them (Figure 7a).
474 We hypothesized that these surface deformations could be induced by fault slip along
475 ENE-dipping normal fault systems (Figure 7).

476

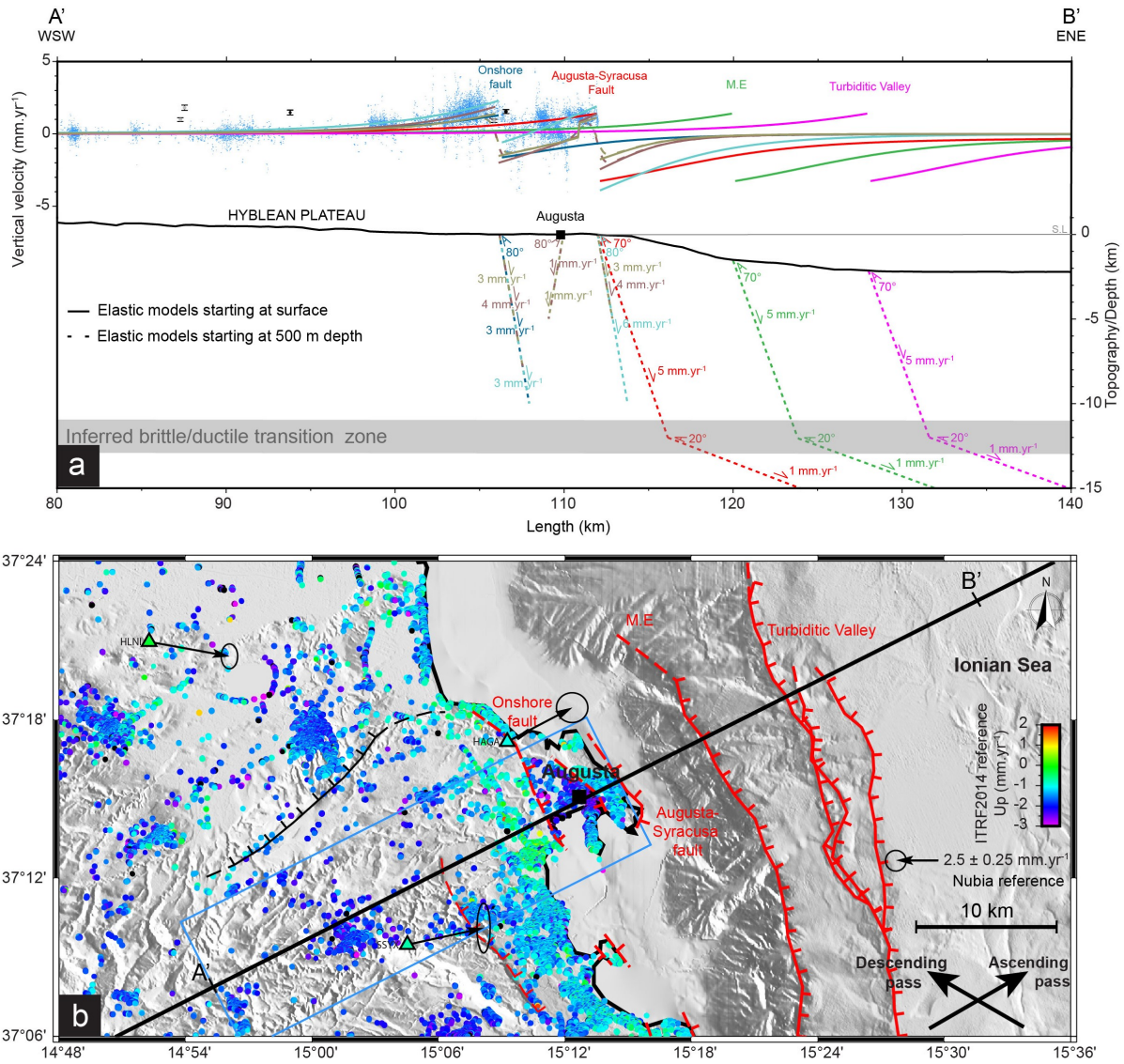


Figure 7 : a) Coulomb 3.4 (Toda et al., 2011) numerical models of interseismic elastic loading (~~step of 100 m~~) on offshore and coastal inferred active faults along the eastern Hyblean Platform. PS-InSAR Up velocities (*in blue*) are stacked across a 5 km width on both sides of the AB profile ~~and appear in blue~~. Modeled interseismic deformations related to: the Turbiditic Valley normal fault (*in magenta*); the Malta Escarpment (*in green*); the Augusta-Siracusa coastal fault (*in red*); onshore inferred active faults in Augusta (*in dark blue*). Modeled elastic loading of the Augusta-Siracusa coastal fault plus onshore inferred active faults in Augusta are represented in light blue, light, and dark brown lines. Topography/depth is represented without vertical exaggeration ($V.E.x1$). b) Map view of geodetic data in the northeastern part of the Hyblean Plateau. Major faults of the Hyblean Plateau including the Augusta-Siracusa coastal fault and the inferred onshore active fault, and Malta Escarpment (M.E) including the Turbiditic Valley faults (red: active fault; red dashed: inferred active fault; black: inferred aseismic slip).

477 The first set of models corresponds to interseismic locking of the shallow (0 to
 478 10-15 km depth) sections of the main normal faults identified in the study area (Figure
 479 7b) and elastic loading by deep (> 15 km depth) creeping sections. Regardless of the
 480 deep fault geometry or slip rates, all these models generate generalized long-wavelength
 481 subsidence rates incompatible with the geodetic data (green dotted line, Supplementary
 482 Figure S13). Thus, we dismiss interseismic loading as a potential mechanism to explain

483 the short wavelength [surface deformation](#) patterns.

484 The second set of models corresponds to shallow aseismic slip [imposed](#) on three
485 offshore normal faults: the Augusta-Siracusa [coastal](#) fault (Bianca et al., 1999), the
486 Malta Escarpment [fault](#), and the Turbiditic [Valley](#) fault (Gutscher et al., 2016; Gam-
487 bino et al., 2021, 2022b) (Figure 7a and Supplementary Figure S13). [We decided to test](#)
488 [the Malta Escarpment fault because it lies between the Turbiditic Valley active fault and](#)
489 [the Augusta-Siracusa fault, for which evidence of activity has been documented by as yet](#)
490 [unpublished sparker lines acquired in the Augusta Bay \(G. Barreca, C. Monaco, personal](#)
491 [communication\).](#) The modeled faults (Figure 7a) share a similar listric geometry with a
492 first fault plane dipping 70°NE and extending from the surface to 12 km depth (inferred
493 brittle/ductile transition zone) and a second one dipping 20°NE and extending from 12
494 to 50 km depth (to limit boundary effects). We imposed slip rates of 5 mm/yr on the
495 first fault plane, based on Meschis et al. (2020) model (Supplementary Figure S13), and
496 1 mm/yr on the second plane to dampen the elastic deformation produced by slip on the
497 shallow fault (Figure 7a). Aseismic slip on these various faults produces coastal uplift
498 rates, reaching at most ~ 1 mm/yr for the Augusta-Siracusa fault, consistent with the
499 PS-InSAR measurements east of Augusta (Figure 7a). However, all the modeled offshore
500 faults failed to reproduce the ~ 2 -3 mm/yr [relative](#) uplift rates measured west of Augusta
501 (Figures 7a and 7b).

502 The third set of models [focuses](#) on surface deformation generated by aseismic creep
503 on 70-80° ENE-dipping shallow [coastal and onshore](#) fault planes. We first simulate slip on
504 the upper portion of the Augusta-Siracusa fault, but [if](#) this model [succeeds](#) in producing
505 sufficient uplift east of Augusta, it [fails](#) to reproduce the [observed](#) relative uplift west of
506 Augusta. Based on PS-InSAR data and structural evidence of [regional](#) onshore normal
507 faulting (e.g., Adam et al., 2000; Gambino et al., 2021), we added to the previous Augusta-
508 Siracusa fault model [an](#) 80° dipping onshore normal fault outcropping at the 106 km mark
509 of the AB profile ([sharp velocity gradient in the PS-InSAR data](#)), with a slip rate of 3
510 mm/yr down to 10 km depth (light blue lines in Figure 7a). The surface deformation
511 generated by this dual creeping fault can explain the observed PS-InSAR relative uplift
512 between the 103 and 106 km profile marks and 110 and 112 km. [Note that](#) imposing
513 aseismic slip on the onshore normal fault alone fails to reproduce the subsidence east of
514 Augusta (dark blue line in Figure 7a).

515 The triangular patterns of sharp steps and associated lows in the PS-InSAR data
516 could be also fitted by a **three-fault** model, involving shallower aseismic creep (up to 5 to
517 8 km depth) and combining the onshore ENE-dipping fault (106 km mark), creeping at
518 3-4 mm/yr, **with** an antithetic onshore WSW-dipping fault (110 km mark), creeping at
519 1 mm/yr, and the Augusta-Siracusa coastal fault (112 km mark), creeping at 3-4 mm/yr
520 (brown lines in Figure 7a). ~~This ad-hoc model illustrates that the short wavelength geode-~~
521 ~~tic signal along the Eastern Hyblean Plateau coast can be explained by ongoing extension~~
522 ~~tectonics and creep on coastal normal faults.~~ We test the same configuration (two onshore
523 faults and the Augusta-Siracusa coastal fault) with a fault plane propagating to the surface
524 up to 500 m depth (Figure 7a). This model, equivalent to a blind fault, induces vertical
525 surface deformation (between the 106 and 110 km marks) about 0.2 mm/yr slower than
526 the model starting to creep from the surface but remains consistent with the PS-InSAR
527 data.

528 All this ad-hoc model, illustrates that the short wavelength geodetic signal along
529 the Eastern Hyblean Plateau coast could be explained by ongoing extension tectonics and
530 creep on coastal normal faults.

531 3.4 Alternative hypothesis

532 To explore ~~if other natural processes hypothesis that~~ could explain part of the
533 observed geodetic velocity patterns, we ~~explore briefly investigate~~ three alternative
534 models:

536 **Mantle flow upwelling**

537
538 Seismic tomography and volcanic data identify a slab window extending along
539 most of the northern coast of Sicily, with a slab break-off recently propagating from
540 west to east and potentially triggering toroidal and upwelling mantle flows (Trua et al.,
541 2003; Civello and Margheriti, 2004; Faccenna et al., 2005; Scarfi et al., 2018). This
542 process could induce long wavelength surface motions (so-called dynamic topography)
543 over the whole Sicily. However, **mantle flow numerical modeling** mainly predicts
544 areas of uplift and subsidence restricted to Mount Etna and the southern Peloritani

545 region (Faccenna et al., 2011; Gallen et al., 2023). Thus, SE Sicily appears to be
546 situated too far from the Ionian slab edge to be affected by upwelling mantle flow. ~~There-~~
547 ~~fore, it is~~ unlikely that ~~this~~ hypothesis explains the observed vertical surface deformations.

548

549 **Volcanic deflation**

550

551 The ~~last most recent major~~ volcanic activity documented on the Hyblean Plateau
552 dates back 1.4 Myr (Schmincke et al., 1997; Behncke, 2004), but recent ~~minor volcanic~~
553 ~~magmatic~~ activity, not recorded at the surface, cannot be ~~totally~~ ruled out. In such a
554 case, volcanic material deflation located below the central Hyblean Plateau could induce
555 local subsidence rates affecting a large region. We tested this hypothesis numerically
556 with deflating spheres, ~~6 to 14 km in diameter~~, (Mogi model, Supplementary Figure
557 S14) situated at a depth of 8 km, at the top of the Paleozoic basement and possible
558 location of magma accumulation (Henriquet et al., 2019). Our first-order tests show
559 that even using extreme deflations of 50-75%, the PS-InSAR subsidence rates cannot
560 be reproduced (Supplementary Figure S14), rendering the volcanic deflation hypothesis
561 extremely unlikely.

562

563 **Hydrological loading**

564

565 The geology of the Hyblean Platform is mainly composed of limestones and
566 dolomites in a karstic environment. Long-term recharge or discharge of karst aquifers
567 is known to induce transient elastic deformation, measurable ~~geodesically with geodetic~~
568 ~~data~~ (e.g., Grillo et al., 2011; Silverii et al., 2016; D’Agostino et al., 2018). ~~Testing this~~
569 ~~hypothesis on the Hyblean Plateau would require data and modeling of the vegetation~~
570 ~~cover, farming activity, bulk volume, soil absorption capacity, etc., which is beyond the~~
571 ~~scope of the present study.~~ Hydrological loading/unloading cycles can have a significant
572 impact on vertical deformation, up to a few tens of millimeters on an annual cycle (White
573 et al., 2022). The effects of hydrological variation on pluri-annual trends are more diffi-
574 cult to assess. Here we consider velocities over 5 years from PS-InSAR and GNSS. The
575 regional subsidence rate of 1-3 mm/yr and associated east-side-down tilt would require
576 an average increase of the water level by $\sim 10-20$ cm over 5 years at the scale of the

577 whole Southeastern Sicily reservoir. This seems incompatible with the absence of similar
578 observable effects over Central and Western Sicily, and with the drought periods that
579 have affected Sicily in recent decades. ~~A detailed analysis of GNSS data could uncover
580 such a hydrological signal, unfortunately, the Hyblean Plateau only comprises 14 GNSS
581 stations, of variable qualities. The best quality stations, NOT1 and HSCI show minimal
582 pluri-annual signals potentially associated with hydrological variations (Supplementary
583 Figures S2 and S4), which cannot explain the long wavelength trend observed over the
584 Hyblean Plateau.~~ Hydrological loading, as a source of large-scale surface subsidence, is
585 then unproved.

586 4 Discussions

587 4.1 Short-term and long-term model limits

588 We explain the eastward tilt and subsidence rates of the Hyblean Plateau as the
589 flexure of the Hyblean continental crust/lithosphere induced by the southward migra-
590 tion of the Calabrian Accretionary Prism (CAP) and retreat of the Ionian subducting
591 slab (sections 3.1 and 3.2). This model is based on the assumption that the geodetic
592 data (GNSS and PS-InSAR), measured over a short period (5-15 years), are represen-
593 tative of the kinematic evolution of the studied region at the scale of a few **hundred**
594 **to a thousand** years. ~~In the absence of significant seismic events during the period of
595 geodetic data acquisition, and considering that major earthquakes ($M > 7$) in SE Sicily
596 probably have a return period of more than 500 years, geodetic data are mainly recording
597 interseismic elastic deformation and possibly, minor permanent one (fault creep, fold-
598 ing, human-related surface deformation).~~ Flexural modeling indicated that the increasing
599 loading of the COT, induced by the southward propagation of the CAP, is not suffi-
600 cient (Figure 6b). The increase in bending force, imposed by a ~ 3 mm/yr southward
601 retreat of the Ionian slab, gives interesting positive results. This process could be strong
602 enough to pull down the Eastern termination of the Hyblean crust at velocities compat-
603 ible with PS-InSAR measurements. However, we obtained this result considering that
604 the Hyblean crust/lithosphere, the **Continent-Ocean Transition (COT)**, and the Ionian
605 crust/lithosphere have similar mechanical properties. **The Alfeo-Etna fault system, in**

606 particular, was considered not mature enough offshore SE Sicily to alter significantly the
 607 mechanical properties of the above-mentioned crustal/lithospheric blocks (Gambino et al.,
 608 2022a). This assumption implies that the COT has a significantly rigid and potentially
 609 too strong rheology (Figure 8), as discussed hereafter (section 4.2).

610 We used simple 2D elastic models based on parameters determined through ana-
 611 lytical modeling of the Ionian oceanic lithosphere flexure using, as a reference, the Ionian
 612 slab geometry determined by Hayes et al. (2018), and data (depth of the top of the Io-
 613 nian crust) extracted from the refraction profiles published in Dellong et al. (2018). The
 614 use of more advanced numerical models (FEM), including 3D modeling methods, would
 615 likely improve our first-order estimates. Similarly, the lateral variations of the Hyblean
 616 continental crust thickness and elastic properties are not accurately known. We used the
 617 available geophysical data (Scarfì et al., 2018; Henriquet et al., 2019), but it was not pos-
 618 sible to constrain the Hyblean crust/lithosphere rheology with better confidence (Figure
 619 8). Should such parameters become available in the future, they could be used to refine
 620 our Hyblean crust/lithosphere flexure calculations.

621 One of the other assumptions we made concerns the rate of increase in the slab
 622 bending force due to the southward propagation of the Ionian slab roll-back. The cal-
 623 culated increase in slab bending force east of the HP is based on the estimated rate of
 624 southward retreat of the Ionian slab defined by the mean of the GNSS NS horizontal ve-
 625 locities in southwest Calabria (using as a reference Malta Island). However, this estimate
 626 may be understated if the Calabrian Arc migrates southward more slowly than the Ionian
 627 slab retreat, due to lateral mechanical interactions with the Apulian and African margins.

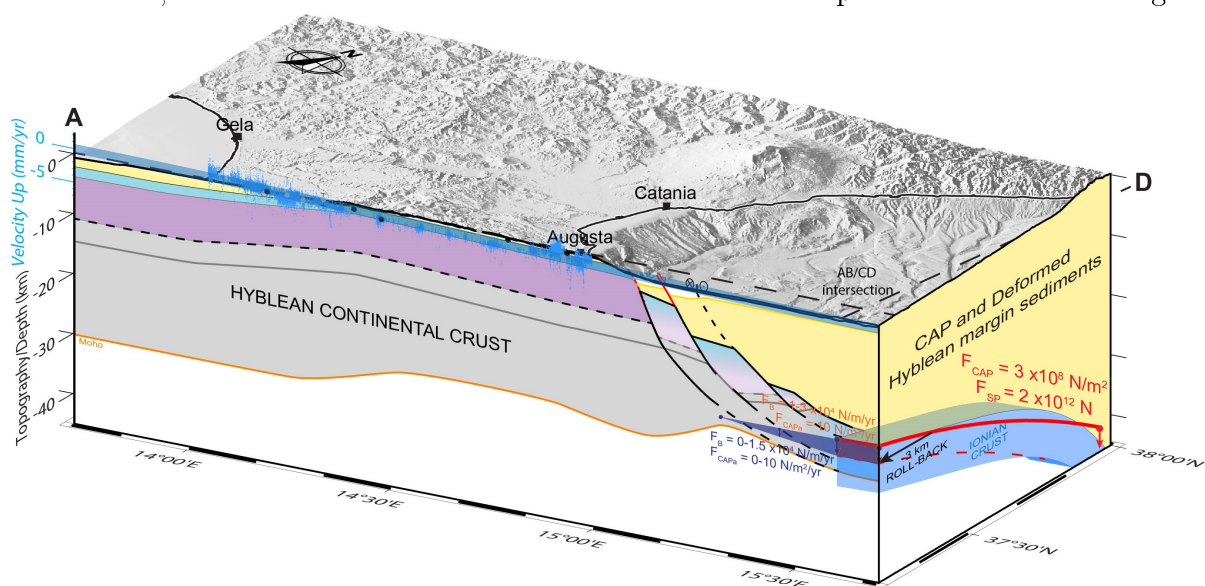


Figure 8 : Schematic 3D deformation model of Southeastern Sicily controlled by Ionian slab roll-back delimited by profiles AB and CD. The 3 km southward retreat of the Ionian crust flexure model (red dashed line) has a horizontal exaggeration of 6 times. The Moho of the Hyblean continental crust determined by geophysical data (Scarfi et al., 2018; Henriquet et al., 2019) is shown in orange. ~~The dashed orange line represents the averaged Moho depth used for flexural modeling calculations. The continent-ocean transition (COT) is shown in purple, and the Calabrian accretionary prism (CAP) and deformed Hyblean margin sediments are shown in yellow. The synthetic structural profile in AB profile have no vertical exaggeration (V.E x1).~~

628 The short-wavelength relative uplift signal, observed in the geodetic data along
629 the Southeastern Sicily coast, must be driven by more shallow deformation mechanisms
630 than those responsible for the long-wavelength eastward flexure of the HP (Figure 6b).
631 Kilometer long surface deformations are typically related to upper crustal deformation
632 processes (e.g., Burgmann and Thatcher, 2013), so we test interseismic loading models on
633 the inferred and identified onshore and offshore fault systems.

634 Slip on the Malta Escarpment and Turbiditic Valley normal fault cannot explain
635 the observed deformation of the eastern coast of the Hyblean Plateau. Only creep on the
636 Augusta-Siracusa coastal fault and the antithetic structure (Bianca et al., 1999; Azzaro
637 and Barbano, 2000) induce onshore vertical deformation compatible with the geodetic
638 data near Augusta. Interseismic slip (creep) on two onshore ENE and WSW 80°-dipping
639 faults, and the Augusta-Siracusa coastal fault fits with the PS-InSAR data in the Eastern
640 of the AB profile. These faults could re-activate inherited Permo-Triassic to Early Jurassic
641 NW-SE extensional structures, leading to the formation of the Augusta Graben, extending
642 up to Siracusa (e.g., Grasso and Lentini, 1982). Even if some seismic activity affects
643 this region (e.g., Adam et al., 2000; Azzaro and Barbano, 2000), field evidence of recent
644 (Holocene) tectonic activity has yet to be demonstrated.

645 Our results suggest that these faults should creep up to the surface or the near-
646 surface (blind fault) to produce sufficient interseismic surface deformation in the footwall.
647 In that later case, their surface expressions could correspond to gentle surface folding or
648 to fold scarp morphologies (e.g., Chen et al., 2007; Li et al., 2015) rather than localized
649 cumulated fault scarps.

650 High precision leveling data acquired between 1970-1991 and analyzed by Spamp-
651 inato et al. (2013), reveals a remarkable ~ 4 mm/yr velocity offset between benchmarks
652 107 and 113, both situated near the coast 5 km west of Augusta (Figure 9c). This sharp
653 vertical velocity gradient is correlated with a marked topographic step, trending NS,

654 and descending toward the sea. Northwest of Augusta, the leveling dataset also shows a
 655 ~ 2 mm/yr offset between benchmarks 119 and 120, associated with a topographic step,
 656 oriented E-W, and facing north (Figures 9b and 9c).

657

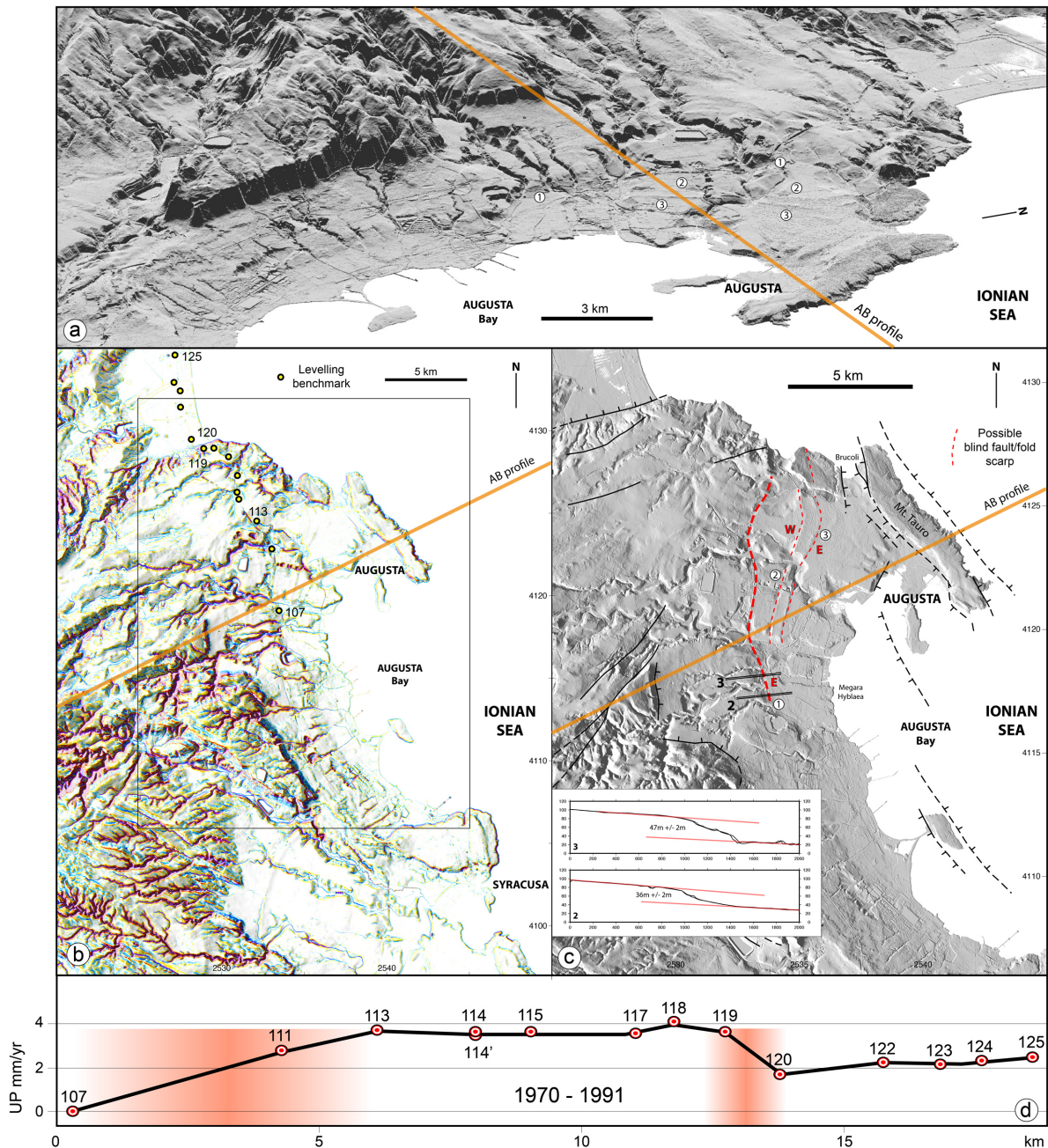


Figure 9 : a) 3D view of a shaded DEM of 2 m resolution from S.I.T.R. regione Siciliana (2013) showing the morphology of the NE part of the Hyblean Plateau. b) Morphological map of the Augusta-Syracusa region showing fluvial incision networks and morphological scarps. The location of leveling benchmarks appears in yellow circles. c) Simplified morpho-structural map highlighting the location of potential tectonic fault/fold scarps in red, and the know fault in thick red dashed line with cross-sections (Supplementary Figure S15). d) 1970-1991 leveling profile (Spampinato et al., 2013) showing a first velocity step (~ 4 mm/yr) between benchmark 107 and 113, and a second one (~ 2 mm/yr), between benchmark 119 and 120 (potential fault zone locations appear in the background in red).

658

A morpho-structural analysis of this region, using a 5 m resolution DEM, out-

659 lines sharp potential drainage incision anomalies oriented perpendicular to the identified
660 topographic steps, potentially related to tectonic surface uplift (Figure 9b). The topo-
661 graphic step between benchmarks 119 and 120 (Figures 9a and 9d) could correspond to
662 the Scordia-Lentini Graben border (e.g., Cultrera et al., 2015). The topographic anomaly
663 between benchmarks 113 and 107, extending to the north up to the Ionian Sea and to
664 the South toward Siracusa, was not previously identified as a tectonic feature. It could
665 correspond to the implemented creeping fault used to match the PS-InSAR data. Up-
666 lifted late Quaternary marine terraces have been evidenced in this region (Bianca et al.,
667 1999; Monaco and Tortorici, 2000; Meschis et al., 2020), but the authors didn't mention
668 a tectonic origin for the measured coastal uplift. Finally, the measured fast surface
669 velocity (1-2 mm/yr) could be considered as inconsistent with the low amplitude of the
670 topographic scarp measurable in the field (a few tens of meters). This point is discussed
671 hereafter (section 4.2).

672 4.2 Combined long-term tectonics and seismic cycle model

673 The subsidence and tilt patterns observed in the geodetic data can be explained
674 by the combination of (1) the flexure of the Hyblean continental crust induced by the
675 bending force generated by the Ionian subduction roll-back (slab-pull) and the CAP
676 overload, explaining the long-wavelength deformation affecting the HP, and (2) the
677 aseismic activity of the Augusta-Siracusa fault system, potentially extending onshore an
678 inferred tectonic structures, explaining the short-wavelength deformation signal affecting
679 the Augusta/Siracusa region (Figure 10). In this section, we discuss how this short-term
680 (geodetic) model could be combined with long-term geological and tectonic observations.

681

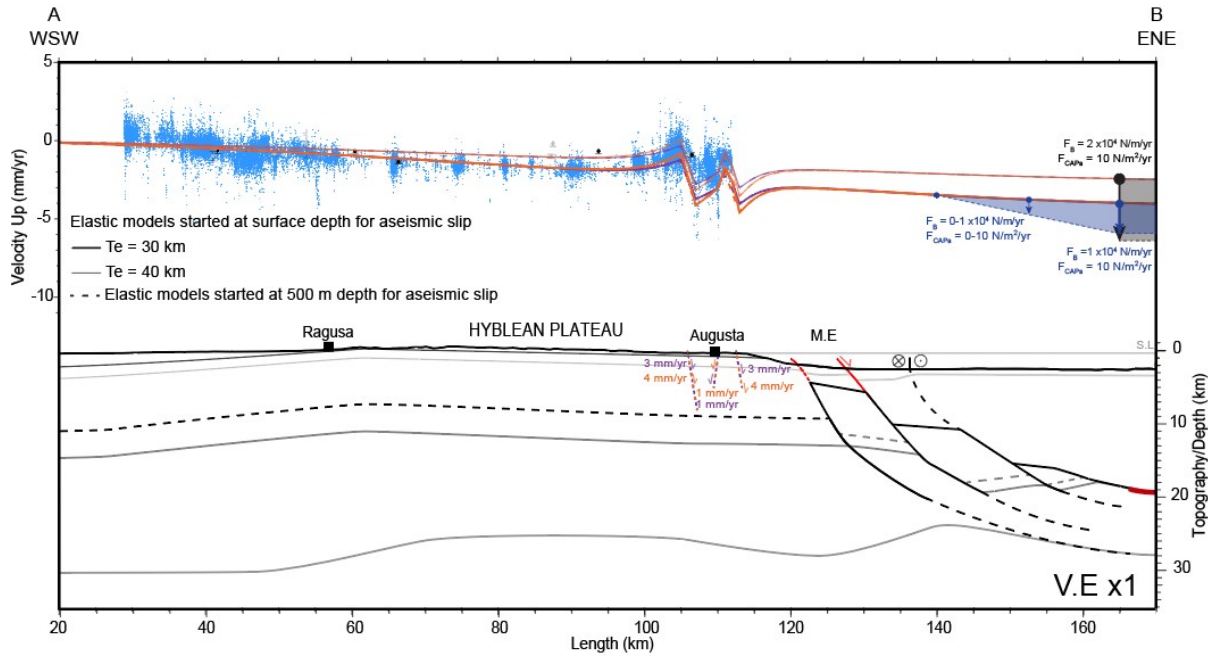


Figure 10 : The final model combining the possible range of the Hyblean continental crust flexural models and the surface deformation (step of 1 km) induced by fault creep (from surface, continuous lines) or active folding in the Augusta-Siracusa coastal domain (from 500 m, dashed lines). In this model, the flexure of the Hyblean continental crust is essentially controlled by the bending force associated with the Ionian slab roll-back (F_B) and, to a lesser extent, by the Calabrian accretionary prism load (F_{CAPa}). The synthetic structural profile (gray) and topography have no vertical exaggeration (V.E.x1).

682 Interestingly, along the N30°E trending AB synthetic profile, a $\sim 1^\circ$ generalized
683 eastward tilting of the HP topography can be evidenced (Figure 4a). The origin of
684 this tilt, in apparent agreement with the geodetic data, could be rather related to the
685 Plio-Quaternary formation of the HP (Henriquet et al., 2019). Indeed, geological analyses
686 suggest that the eastern coast of SE Sicily has been relatively stable over the last million
687 years, with maximal subsidence and uplift amplitudes of ± 0.2 mm/yr (Ferranti et al.,
688 2006). More recently, dating of Late Quaternary marine terraces along the Siracusa-
689 Augusta coastal domain indicates that the eastern coast of the Hyblean Plateau has
690 experienced a slow constant uplift during the last 500 Kyr, increasing northward from 0.1
691 to 0.4 mm/yr (Meschis et al., 2020). On a shorter historical time scale based on Roman
692 archaeological site studies, Scicchitano et al. (2008), propose that the Siracusa coast has
693 been slowly uplifting during the last 4 Kyr, albeit with significant uncertainties. These
694 long-term observations, extending from the Quaternary to historical time, point to a slow
695 regional uplift, apparently in contradiction with the geodetic data. **However, it should be**
696 **remembered that we have considered that PS-InSAR measurements primarily document**
697 **the interseismic phase. As this stage, the part of the seismic cycle that generates uplift**

698 has not yet been taken into account. Previous calculations (Meschis et al., 2020) shown
 699 that a Mw=7 on the active fault of the Malta Escarpment generate little to no coastal
 700 uplift but early and late post-seismic deformation was not taken into consideration.
 701 In addition, a 500 yr seismic cycle contains other earthquakes contributing to surface
 702 deformation than a single M=7 event. To reconcile long and short-time scale surface
 703 motions, we propose an original seismic cycle model driven by the southward roll-back of
 704 the Ionian subduction (Figure 11).

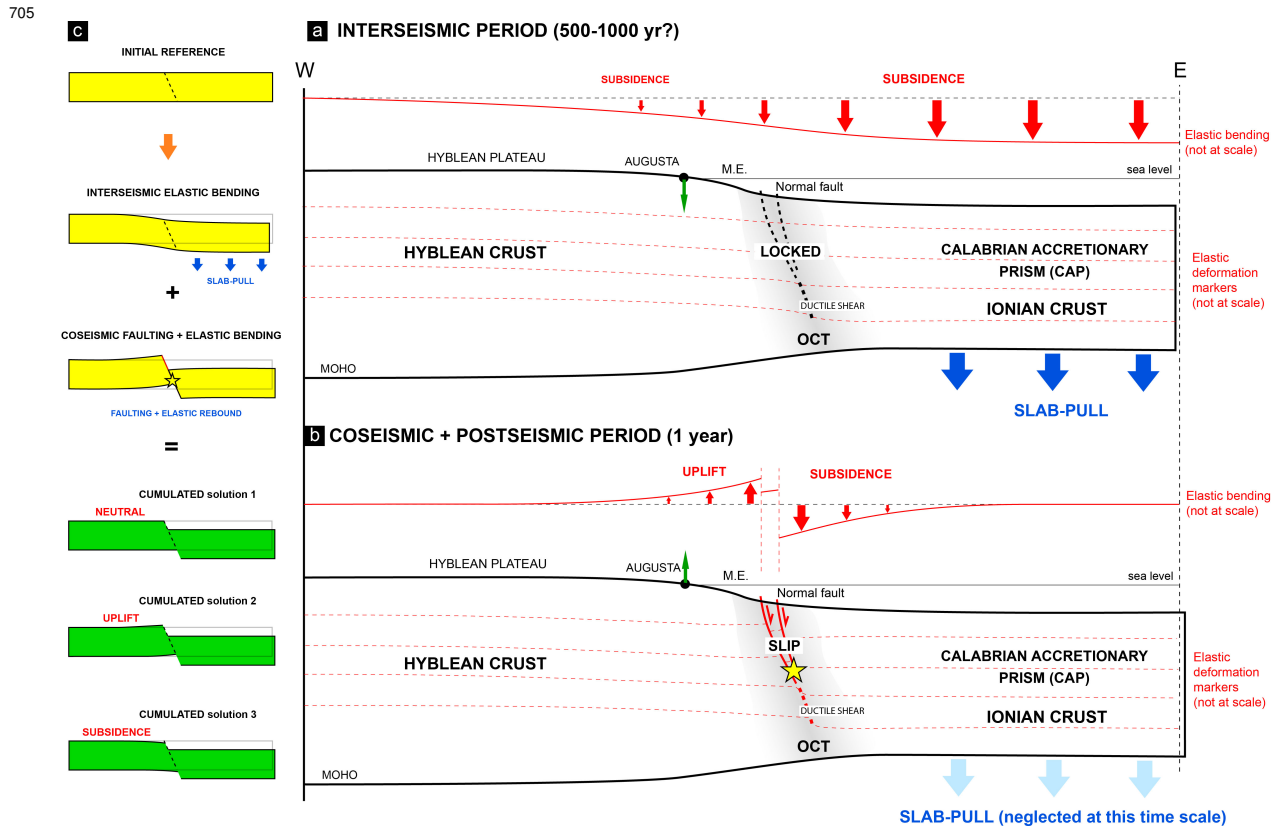


Figure 11 : Schematic model of seismic cycle for south-eastern Sicily, integrating crustal elastic bending, aseismic, and seismic faulting controlled by slab-pull. a) Interseismic period, b) coseismic and postseismic period, c) different scenarios of the cumulated interseismic, postseismic, and coseismic. This model could reconcile short and long-term observations.

706 During the interseismic phase, the active ~~onshore and~~ offshore normal faults affect-
 707 ing the eastern HP and Malta Escarpment are locked. The Hyblean and Ionian crusts
 708 are coupled and can be compared to an elastic beam, bending eastward in response to
 709 an increasing downward vertical force: the slab pull induced by the Ionian slab roll-back
 710 (Figure 11a). Considering a minimum 500-yr return period for major earthquakes such as
 711 the 1693 Val-di-Noto event (Bianca et al., 1999; Meschis et al., 2020) and extrapolating the
 712 PS-InSAR measurements over this period, coastal subsidence along the Siracusa-Augusta
 713 region could reach 1-2 m. This subsidence could be dampened to 0.5-1 m significantly

714 reduced if, at the same time, the onshore faults, potentially related to extrados deforma-
715 tion, creep aseismically ~~during that period~~. During the coseismic ~~and postseismic~~ phase,
716 the offshore ~~Malta Escarpment~~ fault unlocks, and seismic slip induces (for a $M_w > 7$ earth-
717 quake) multi-metric subsidence of the hanging wall and an associated decimetric to metric
718 uplift of the footwall (e.g., Wells and Coppersmith, 1994) (Figure 11b).

719 The cumulated succession of inter-seismic coastal subsidence and co-seismic uplift
720 could result in three different scenarios (Figure 11c). If the co-seismic coastal uplift equals
721 the cumulated interseismic subsidence, the coastal domain remains stable in the long term.
722 If the former is lower than the latter, as predicted by elastic modeling (Figure 7a), the
723 coast subsides. Conversely, long-term coastal uplift occurs if coseismic uplift surpasses
724 interseismic subsidence. Considering that geological data suggest a slow coastal uplift,
725 this last scenario should be preferred, but additional sources of foot-wall uplift should be
726 identified (Ferranti et al., 2006; Meschis et al., 2020). At this stage, we can only evoke
727 raw hypothesis:

- 728 • The buoyancy of the flexed Hyblean crust could significantly increase post-seismic
729 slip after major earthquakes and thus increase footwall uplift in the coastal region.
- 730 • Further north along the coast, the Ionian slab plunges to great depth and is certainly
731 detached from the Hyblean continental margin owing to a tear-fault propagation
732 southward (e.g., Gutscher et al., 2016; Maesano et al., 2020), which could generate
733 additional stress affecting the surface deformation of the studied region.
- 734 • The ~~inferred interseismic activity of the inferred~~ extrados deformation, affecting the
735 coastal domain, ~~onshore faults alone~~ could explain the slow long-term uplift (0.1-0.4
736 mm/yr) off the eastern coast of the HP (e.g., Meschis et al., 2020). In that case,
737 extrados deformation activity should be intermittent, alternating between aseismic
738 fault slip/folding (as presently) and long periods of quiescence. Such a scenario
739 remains speculative and needs to be mechanically tested.
- 740 • Finally, the potential impact of major subduction earthquake along the Calabrian
741 Arc on SE Sicily could be also considered (e.g., Gutscher et al., 2016; Carafa et al.,
742 2018)

5 Conclusion

Present-day deformation of Southeastern Sicily (Hyblean Plateau) reveals specific long and short-wavelength signals indicating a generalized eastward tilting, reversing a few kilometers before reaching the eastern coast of the Hyblean Plateau.

We propose that the long-wavelength tilt and subsidence can be explained by the flexure of the Hyblean continental crust in response to the bending force induced by the southward retreat of the Ionian subduction. Simple flexural modeling, using standard parameters (elastic thickness of 25-40 km, accretionary prism loading of 5-10 N/m²/yr, and a local increase of bending force of $1-3 \times 10^4$ N/m/yr or gradually of 0 to $1-1.5 \times 10^4$ N/m/yr) support this interpretation.

We show that the short wavelength relative coastal uplift, measured geodetically, could be explained by ongoing shallow creep (at 1-4 mm/yr) on ENE trending and steeply dipping normal faults, related to extrado deformation. Some morphologic evidence of surface deformation, correlated with leveling data indicating differential surface uplift, seems to corroborate this hypothesis. However, at this stage, the extrado deformation hypothesis has yet to be validated. We investigated other hypotheses, such as upwelling mantle flow, volcanic deflation, and hydrological loading, and found them to be much less plausible.

Finally, we propose an original seismic cycle model in which the surface deformation of Southeastern Sicily is mainly controlled by bending force induced by the Ionian slab roll-back, tilting the Hyblean Plateau eastward. The bending of the continental crust causes aseismic extrados deformation along the eastern coast of the Hyblean Plateau while the normal faults, affecting the continent-ocean transition, potentially at the origin of the 1693 earthquake, remain currently locked and accumulating interseismic strain. During a major earthquake, the coastal domain uplifts and compensates for the interseismic subsidence.

To further develop the formulated hypotheses, the acquisition of additional data is required mandatory, such as new high-resolution bathymetric data, onshore and offshore high-resolution seismic data (CHIRP), and on-site analysis to investigate inferred coastal active faults along the Augusta-Siracusa region. Besides, acquiring new PS-InSAR data would improve distinguishing geological processes from human activities. To further

774 ~~investigate these assumptions~~, It will be also of interest to perform more advanced
775 flexural models using 3D finite element modeling techniques. ~~and perform electrical~~
776 ~~resistivity profile and gravimetric measurements to better constrain karstic aquifers~~
777 ~~and the potential role of deep water storage and discharge on vertical surface deformation.~~

778

779 **Competing interest:** The first author and co-authors have declared none competing
780 interests.

781 **Acknowledgments:** This study was funded by the CNRS-INSU-Tellus programs, and
782 the University of Montpellier (UM). Data supporting materials can be download from the
783 Easy Data repository (Dataterra (easydata.earth)). The maps and graphics presented in
784 this study were generated using the Generic Mapping Tools (GMT) software (Wessel and
785 Smith, 1998). We are grateful to Serge Lallemand and Nestor Cerpa for helpful discussions
786 on [subduction zone dynamics and flexural modeling](#).

787 **Author contributions:**

788 Data curation: Amélie Viger, Stéphane Dominguez

789 Formal analysis: Amélie Viger, Stéphane Dominguez, Michel Peyret, Stéphane Mazzotti,
790 Maxime Henriquet, Giovanni Barreca, Carmelo Monaco, Adrien Damon

791 Funding acquisition: Stéphane Dominguez

792 Resources: Amélie Viger, Stéphane Dominguez, Maxime Henriquet, Giovanni Barreca,
793 Carmelo Monaco

794 Software: Amélie Viger, Adrien Damon, Michel Peyret, Stéphane Mazzotti

795 Visualization: Amélie Viger, Stéphane Dominguez

796 Writing – original draft: Amélie Viger, Stéphane Dominguez

797 Writing – review and editing: Amélie Viger, Stéphane Dominguez, Michel Peyret,
798 Stéphane Mazzotti, Maxime Henriquet, Giovanni Barreca, Carmelo Monaco, Adrien Da-
799 mon

800 References

801 Adam, J., Reuther, C. D., Grasso, M., and Torelli, L.: Active fault kinematics and crustal
802 stresses along the Ionian margin of southeastern Sicily, *Tectonophysics*, 326, 217–239,
803 [https://doi.org/10.1016/S0040-1951\(00\)00141-4](https://doi.org/10.1016/S0040-1951(00)00141-4), 2000.

804 Afilhado, A., Moulin, M., Aslanian, D., Schnürle, P., Klingelhoefer, F., Nouzé, H., Ra-
805 bineau, M., Leroux, E., and Beslier, M.-O.: Deep crustal structure across a young

806 passive margin from wide-angle and reflection seismic data (The SARDINIA Experiment)
807 – II. Sardinia’s margin, *Bulletin de la Société Géologique de France*, 186, 331–351,
808 <https://doi.org/10.2113/gssgfbull.186.4-5.331>, 2015.

809 Almeida, J., Riel, N., Rosas, F. M., Duarte, J. C., and Schellart,
810 W. P.: Polarity-reversal subduction zone initiation triggered by buoyant
811 plateau obstruction, *Earth and Planetary Science Letters*, 577, 117–195,
812 <https://www.sciencedirect.com/science/article/pii/S0012821X21004507>,
813 publisher: Elsevier, 2022.

814 Altamimi, Z., Rebischung, P., Métivier, L., and Collilieux, X.: ITRF2014: A new re-
815 lease of the International Terrestrial Reference Frame modeling nonlinear station mo-
816 tions, *Journal of Geophysical Research: Solid Earth*, 121, 6109–6131, [https://doi.org/](https://doi.org/10.1002/2016JB013098)
817 [10.1002/2016JB013098](https://doi.org/10.1002/2016JB013098), 2016.

818 Anzidei, M., Scicchitano, G., Scardino, G., Bignami, C., Tolomei, C., Vecchio, A., Ser-
819 pelloni, E., De Santis, V., Monaco, C., Milella, M., Piscitelli, A., and Mastronuzzi, G.:
820 Relative Sea-Level Rise Scenario for 2100 along the Coast of South Eastern Sicily (Italy)
821 by InSAR Data, *Satellite Images and High-Resolution Topography, Remote Sensing*,
822 13, 1108, <https://doi.org/10.3390/rs13061108>, 2021.

823 APAT: Carta geologica d’Italia Scala 1: 1 250 000,
824 <https://www.isprambiente.gov.it/images/progetti/progetto-1250-ita.jpg>,
825 2005.

826 Argnani, A.: Commentary: Deformation Pattern of the Northern Sector of the Malta
827 Escarpment (Offshore SE Sicily, Italy): Fault Dimension, Slip Prediction, and Seis-
828 motectonic Implications, *Frontiers in Earth Science*, 9, 770–364, [https://doi.org/](https://doi.org/10.3389/feart.2021.770364)
829 [10.3389/feart.2021.770364](https://doi.org/10.3389/feart.2021.770364), 2021.

830 Argnani, A. and Bonazzi, C.: Malta Escarpment fault zone offshore eastern Sicily:
831 Pliocene-Quaternary tectonic evolution based on new multichannel seismic data, *Tec-
832 tonics*, 24, <https://doi.org/10.1029/2004TC001656>, 2005.

833 Argnani, A., Armigliato, A., Pagnoni, G., Zaniboni, F., Tinti, S., and Bonazzi, C.: Active
834 tectonics along the submarine slope of south-eastern Sicily and the source of the 11
835 January 1693 earthquake and tsunamis, *Natural Hazards and Earth System Sciences*,
836 12, 1311–1319, <https://doi.org/10.5194/nhess-12-1311-2012>, 2012.

837 Azzaro, R. and Barbano, M. S.: Analysis of the seismicity of Southeastern Sicily: a pro-
838 posed tectonic interpretation, <https://www.earth-prints.org/handle/2122/1292>,
839 2000.

840 Behncke, B.: Late Pliocene volcanic island growth and flood basalt-like lava emplacement
841 in the Hyblean Mountains (SE Sicily): LATE PLIOCENE HYBLEAN VOLCAN-
842 ISM, *Journal of Geophysical Research: Solid Earth*, 109, n/a–n/a, [https://doi.org/](https://doi.org/10.1029/2003JB002937)
843 [10.1029/2003JB002937](https://doi.org/10.1029/2003JB002937), 2004.

844 Bianca, M., Monaco, C., Tortorici, L., and Cernobori, L.: Quaternary normal faulting in
845 southeastern Sicily (Italy): a seismic source for the 1693 large earthquake, *Geophysical
846 Journal International*, 139, 370–394, <https://doi.org/10.1046/j.1365-246x.1999.00942.x>,
847 1999.

848 Bigi, G., Cosentino, D., Parlotto, M., and Sartori, R.: Structural model of Italy, sheet 6,
849 1991, National Council of Researches Roma, 1991.

850 Blewitt, G., Hammond, W., and Kreemer, C.: Harnessing the GPS Data Explosion for
851 Interdisciplinary Science, *Eos*, 99, <https://doi.org/10.1029/2018eo104623>, 2018.

- 852 Burgmann, R. and Thatcher, W.: Space geodesy: A revolution in crustal deformation
853 measurements of tectonic processes, Special Paper of the Geological Society of America,
854 500, 397–430, [https://doi.org/10.1130/2013.2500\(12\)](https://doi.org/10.1130/2013.2500(12)), 2013.
- 855 Canova, F., Tolomei, C., Salvi, S., Toscani, G., and Seno, S.: Land subsidence along
856 the Ionian coast of SE Sicily (Italy), detection and analysis via Small Baseline Subset
857 (SBAS) multitemporal differential SAR interferometry: LAND SUBSIDENCE ALONG
858 THE IONIAN COAST OF SE SICILY (ITALY), *Earth Surface Processes and Land-*
859 *forms*, 37, 273–286, <https://doi.org/10.1002/esp.2238>, 2012.
- 860 Carafa, M. M. C., Kastelic, V., Bird, P., Maesano, F. E., and Valensise, G.: A “Geodetic
861 Gap” in the Calabrian Arc: Evidence for a Locked Subduction Megathrust?, *Geophys-*
862 *ical Research Letters*, 45, 1794–1804, <https://doi.org/10.1002/2017GL076554>, _eprint:
863 <https://onlinelibrary.wiley.com/doi/pdf/10.1002/2017GL076554>, 2018.
- 864 Carminati, E. and Doglioni, C.: Mediterranean Tectonics, in: *Encyclopedia of Geology*,
865 pp. 135–146, <https://doi.org/10.1016/B0-12-369396-9/00135-0>, 2005.
- 866 Carminati, E., Lustrino, M., and Doglioni, C.: Geodynamic evolution of the central and
867 western Mediterranean: Tectonics vs. igneous petrology constraints, *Tectonophysics*,
868 579, 173–192, <https://doi.org/10.1016/j.tecto.2012.01.026>, 2012.
- 869 Catalano, R., Doglioni, C., and Merlini, S.: On the Mesozoic Ionian Basin, *Geophysical*
870 *Journal International*, 144, 49–64, <https://doi.org/10.1046/j.0956-540X.2000.01287.x>,
871 2001.
- 872 Chen, Y.-G., Lai, K.-Y., Lee, Y.-H., Suppe, J., Chen, W.-S., Lin, Y.-N. N., Wang, Y.,
873 Hung, J.-H., and Kuo, Y.-T.: Coseismic fold scarps and their kinematic behavior in the
874 1999 Chi-Chi earthquake Taiwan, *Journal of Geophysical Research: Solid Earth*, 112,
875 <https://doi.org/10.1029/2006JB004388>, 2007.
- 876 Civello, S. and Margheriti, L.: Toroidal mantle flow around the Calabrian slab (Italy) from
877 SKS splitting: TOROIDAL FLOW AROUND THE CALABRIAN SLAB, *Geophysical*
878 *Research Letters*, 31, n/a–n/a, <https://doi.org/10.1029/2004GL019607>, 2004.
- 879 Cloetingh, S., Ziegler, P., Beekman, F., Burov, E., Garcia-Castellanos, D., and Matenco,
880 L.: Tectonic Models for the Evolution of Sedimentary Basins, in: *Treatise on Geo-*
881 *physics*, pp. 513–592, Elsevier, ISBN 978-0-444-53803-1, [https://doi.org/10.1016/B978-](https://doi.org/10.1016/B978-0-444-53802-4.00117-2)
882 [0-444-53802-4.00117-2](https://doi.org/10.1016/B978-0-444-53802-4.00117-2), 2015.
- 883 Cultrera, F., Barreca, G., Scarfi, L., and Monaco, C.: Fault reactivation by
884 stress pattern reorganization in the Hyblean foreland domain of SE Sicily (Italy)
885 and seismotectonic implications, *Tectonophysics*, 661, 215–228, <https://doi.org/10.1016/j.tecto.2015.08.043>, 2015.
- 887 D’Agostino, N., D’Anastasio, E., Gervasi, A., Guerra, I., Nedimović, M. R., See-
888 ber, L., and Steckler, M.: Forearc extension and slow rollback of the Calabrian
889 Arc from GPS measurements, *Geophysical Research Letters*, 38, <https://doi.org/10.1029/2011GL048270>, 2011.
- 891 D’Agostino, N., Silverii, F., Amoroso, O., Convertito, V., Fiorillo, F., Ventafriidda, G., and
892 Zollo, A.: Crustal Deformation and Seismicity Modulated by Groundwater Recharge
893 of Karst Aquifers, *Geophysical Research Letters*, 45, 12,253–12,262, <https://doi.org/10.1029/2018GL079794>, 2018.
- 895 Dellong, D., Klingelhoefer, F., Kopp, H., Graindorge, D., Margheriti, L., Moretti, M.,
896 Murphy, S., and Gutscher, M.-A.: Crustal Structure of the Ionian Basin and Eastern

- 897 Sicily Margin: Results From a Wide-Angle Seismic Survey, *Journal of Geophysical*
898 *Research: Solid Earth*, 123, 2090–2114, <https://doi.org/10.1002/2017JB015312>, 2018.
- 899 Dellong, D., Klingelhoefer, F., Dannowski, A., Kopp, H., Murphy, S., Graindorge, D.,
900 Margheriti, L., Moretti, M., Barreca, G., Scarfi, L., Polonia, A., and Gutscher, M.-A.:
901 Geometry of the Deep Calabrian Subduction (Central Mediterranean Sea) From Wide-
902 Angle Seismic Data and 3-D Gravity Modeling, *Geochemistry, Geophysics, Geosystems*,
903 21, 2019GC008 586, <https://doi.org/10.1029/2019GC008586>, 2020.
- 904 Faccenna, C., Becker, T. W., Lucente, F. P., Jolivet, L., and Rossetti, F.: History of
905 subduction and back-arc extension in the Central Mediterranean, *Geophysical Journal*
906 *International*, 145, 809–820, <https://doi.org/10.1046/j.0956-540x.2001.01435.x>, 2001.
- 907 Faccenna, C., Civetta, L., D’Antonio, M., Funicello, F., Margheriti, L., and Piro-
908 mallo, C.: Constraints on mantle circulation around the deforming Calabrian slab,
909 *Geophysical Research Letters*, 32, <https://doi.org/10.1029/2004GL021874>,
910 [_eprint:
https://onlinelibrary.wiley.com/doi/pdf/10.1029/2004GL021874](https://onlinelibrary.wiley.com/doi/pdf/10.1029/2004GL021874), 2005.
- 911 Faccenna, C., Molin, P., Orecchio, B., Olivetti, V., Bellier, O., Funicello, F., Minelli,
912 L., Piro mallo, C., and Billi, A.: Topography of the Calabria subduction zone (southern
913 Italy): Clues for the origin of Mt. Etna, *Tectonics*, 30, 2010TC002 694, [https://doi.org/
914 10.1029/2010TC002694](https://doi.org/10.1029/2010TC002694), 2011.
- 915 Ferranti, L., Antonioli, F., Mauz, B., Amorosi, A., Dai Pra, G., Mastronuzzi, G.,
916 Monaco, C., Orrù, P., Pappalardo, M., Radtke, U., Renda, P., Romano, P., Sansò,
917 P., and Verrubbi, V.: Markers of the last interglacial sea-level high stand along
918 the coast of Italy: Tectonic implications, *Quaternary International*, 145-146, 30–54,
919 <https://doi.org/10.1016/j.quaint.2005.07.009>, 2006.
- 920 Ferranti, L., Antonioli, F., Anzidei, M., Monaco, C., and Stocchi, P.: The timescale
921 and spatial extent of recent vertical tectonic motions in Italy: insights from rela-
922 tive sea-level changes studies, *Journal of the Virtual Explorer*, 36, [https://doi.org/
923 10.3809/jvirtex.2010.00255](https://doi.org/10.3809/jvirtex.2010.00255), 2010.
- 924 Finetti, I. R., Lentini, F., Carbone, S., Del Ben, A., Di Stefano, A., Forlin, E., Guarnieri,
925 P., Pipan, M., and Prizzon, A.: Geological outline of Sicily and lithospheric tectono-
926 dynamics of its Tyrrhenian margin from new CROP seismic data, *CROP Project: deep*
927 *seismic exploration of the central Mediterranean and Italy*, pp. 319–375, 2005.
- 928 Frizon De Lamotte, D., Raulin, C., Mouchot, N., Wrobel-Daveau, J.-C., Blanpied, C., and
929 Ringenbach, J.-C.: The southernmost margin of the Tethys realm during the Mesozoic
930 and Cenozoic: Initial geometry and timing of the inversion processes, *Tectonics*, 30,
931 2010TC002 691, <https://doi.org/10.1029/2010TC002691>, 2011.
- 932 Funicello, R., Parotto, M., Praturlon, A., and Bigi, G.: Carta tettonica d’Italia alla scala
933 1: 1.500. 000, *CNR Progetto Finalizzato Geodinamica*, Pubbl, 269, 1981.
- 934 Gallen, S. F., Seymour, N. M., Glotzbach, C., Stockli, D. F., and O’Sullivan, P.: Calabrian
935 forearc uplift paced by slab–mantle interactions during subduction retreat, *Nature Geo-*
936 *science*, pp. 1–8, 2023.
- 937 Gambino, S., Barreca, G., Gross, F., Monaco, C., Krastel, S., and Gutscher, M.-A.: De-
938 formation Pattern of the Northern Sector of the Malta Escarpment (Offshore SE Sicily,
939 Italy): Fault Dimension, Slip Prediction, and Seismotectonic Implications, *Frontiers in*
940 *Earth Science*, 8, 594 176, <https://doi.org/10.3389/feart.2020.594176>, 2021.
- 941 Gambino, S., Barreca, G., Bruno, V., De Guidi, G., Ferlito, C., Gross, F., Mat-
942 tia, M., Scarfi, L., and Monaco, C.: Transtension at the Northern Termina-

- 943 tion of the Alfeo-Etna Fault System (Western Ionian Sea, Italy): Seismotec-
944 tonic Implications and Relation with Mt. Etna Volcanism, *Geosciences*, 12, 128,
945 <https://www.mdpi.com/2076-3263/12/3/128>, publisher: MDPI, 2022a.
- 946 Gambino, S., Barreca, G., Gross, F., Monaco, C., Gutscher, M.-A., and Alsop, G. I.:
947 Assessing the rate of crustal extension by 2D sequential restoration analysis: A case
948 study from the active portion of the Malta Escarpment, *Basin Research*, 34, 321–341,
949 <https://doi.org/10.1111/bre.12621>, 2022b.
- 950 Goes, S., Giardini, D., Jenny, S., Hollenstein, C., Kahle, H. G., and Geiger, A.: A
951 recent tectonic reorganization in the south-central Mediterranean, *Earth and Planetary
952 Science Letters*, 226, 335–345, <https://doi.org/10.1016/j.epsl.2004.07.038>, 2004.
- 953 Grasso, M. t. and Lentini, F.: Sedimentary and tectonic evolution of the eastern Hyblean
954 Plateau (southeastern Sicily) during late Cretaceous to Quaternary time, *Palaeogeog-
955 raphy, Palaeoclimatology, Palaeoecology*, 39, 261–280, 1982.
- 956 Grillo, B., Braitenberg, C., Devoti, R., and Nagy, I.: The study of karstic aquifers by
957 geodetic measurements in Bus de la Genziana station – Cansiglio plateau (Northeastern
958 Italy), *Acta Carsologica*, 40, <https://doi.org/10.3986/ac.v40i1.35>, 2011.
- 959 Gueguen, E., Doglioni, C., and Fernandez, M.: On the post-25 Ma geodynamic evo-
960 lution of the western Mediterranean, *Tectonophysics*, 298, 259–269, [https://doi.org/
961 10.1016/S0040-1951\(98\)00189-9](https://doi.org/10.1016/S0040-1951(98)00189-9), 1998.
- 962 Gutscher, M.-A., Roger, J., Baptista, M.-A., Miranda, J. M., and Tinti, S.: Source
963 of the 1693 Catania earthquake and tsunami (southern Italy): New evidence from
964 tsunami modeling of a locked subduction fault plane, *Geophysical Research Letters*,
965 33, <https://doi.org/10.1029/2005GL025442>, 2006.
- 966 Gutscher, M.-A., Dominguez, S., de Lepinay, B. M., Pinheiro, L., Gallais, F., Babonneau,
967 N., Cattaneo, A., Le Faou, Y., Barreca, G., Micalef, A., and Rovere, M.: Tectonic
968 expression of an active slab tear from high-resolution seismic and bathymetric data off-
969 shore Sicily (Ionian Sea), *Tectonics*, 35, 39–54, <https://doi.org/10.1002/2015TC003898>,
970 2016.
- 971 Handy, M. R., M. Schmid, S., Bousquet, R., Kissling, E., and Bernoulli, D.: Recon-
972 ciling plate-tectonic reconstructions of Alpine Tethys with the geological–geophysical
973 record of spreading and subduction in the Alps, *Earth-Science Reviews*, 102, 121–158,
974 <https://doi.org/10.1016/j.earscirev.2010.06.002>, 2010.
- 975 Handy, M. R., Ustaszewski, K., and Kissling, E.: Reconstructing the
976 Alps–Carpathians–Dinarides as a key to understanding switches in subduction
977 polarity, slab gaps and surface motion, *International Journal of Earth Sciences*, 104,
978 1–26, <https://doi.org/10.1007/s00531-014-1060-3>, 2015.
- 979 Hayes, G. P., Moore, G. L., Portner, D. E., Hearne, M., Flamme, H., Furtney, M., and
980 Smoczyk, G. M.: Slab2, a comprehensive subduction zone geometry model, *Science*,
981 362, 58–61, <https://doi.org/10.1126/science.aat4723>, 2018.
- 982 Henriquet, M., Dominguez, S., Barreca, G., Malavieille, J., Cadio, C., and
983 Monaco, C.: Deep Origin of the Dome-Shaped Hyblean Plateau, Southeastern
984 Sicily: A New Tectono-Magmatic Model, *Tectonics*, 38, 4488–4515, [https://doi.org/
985 10.1029/2019TC005548](https://doi.org/10.1029/2019TC005548), 2019.
- 986 Henriquet, M., Dominguez, S., Barreca, G., Malavieille, J., and Monaco, C.: Struc-
987 tural and tectono-stratigraphic review of the Sicilian orogen and new insights

- 988 from analogue modeling, *Earth-Science Reviews*, 208, 103–257, [https://doi.org/](https://doi.org/10.1016/j.earscirev.2020.103257)
989 10.1016/j.earscirev.2020.103257, 2020.
- 990 Henriquet, M., Peyret, M., Dominguez, S., Barreca, G., Monaco, C., and Mazzotti, S.:
991 Present-Day Surface Deformation of Sicily Derived From Sentinel-1 InSAR Time-Series,
992 *Journal of Geophysical Research: Solid Earth*, 127, e2021JB023071, [https://doi.org/](https://doi.org/10.1029/2021JB023071)
993 10.1029/2021JB023071, 2022.
- 994 Istituto Nazionale di Geofisica e Vulcanologia (INGV): Rete Sismica Nazionale (RSN),
995 pp. approx. 27 GB per day of new waveform data, approx. 415 active seismic sta-
996 tions, the archive totals to more than 600 distinct seismic stations, [https://doi.org/](https://doi.org/10.13127/SD/X0FXNH7QFY)
997 10.13127/SD/X0FXNH7QFY, 2005.
- 998 Jolivet, L.: Tethys and Apulia (Adria), 100 years of reconstructions, *Comptes Rendus.*
999 *Géoscience*, 355, 9–28, <https://doi.org/10.5802/crgeos.198>, 2023.
- 1000 Klingelhoefer, F., Déverchère, J., Graindorge, D., Aïdi, C., Badji, R., Bouyahiaoui, B.,
1001 Leprêtre, A., Mihoubi, A., Beslier, M.-O., Charvis, P., Schnurle, P., Sage, F., Medaouri,
1002 M., Arab, M., Bracene, R., Yelles-Chaouche, A., Badsì, M., Galvé, A., and Géli, L.: For-
1003 mation, segmentation and deep crustal structure variations along the Algerian margin
1004 from the SPIRAL seismic experiment, *Journal of African Earth Sciences*, 186, 104–133,
1005 <https://doi.org/10.1016/j.jafrearsci.2021.104433>, 2022.
- 1006 Kreemer, C., Blewitt, G., and Klein, E. C.: A geodetic plate motion and Global Strain
1007 Rate Model, *Geochemistry, Geophysics, Geosystems*, 15, 3849–3889, [https://doi.org/](https://doi.org/10.1002/2014GC005407)
1008 10.1002/2014GC005407, 2014.
- 1009 Lallemand, S., Heuret, A., Faccenna, C., and Funiciello, F.: Subduction dynamics as
1010 revealed by trench migration: SUBDUCTION DYNAMICS, *Tectonics*, 27, n/a–n/a,
1011 <https://doi.org/10.1029/2007TC002212>, 2008.
- 1012 Lentini, F. and Carbone, S.: Geologia della Sicilia-geology of Sicily, *Memorie Descr. Carta*
1013 *Geologica d’Italia*, 95, 7–414, 2014.
- 1014 Levandowski, W., Herrmann, R. B., Briggs, R., Boyd, O., and Gold, R.: An updated
1015 stress map of the continental United States reveals heterogeneous intraplate stress,
1016 *Nature Geoscience*, 11, 433–437, <https://doi.org/10.1038/s41561-018-0120-x>, 2018.
- 1017 Li, T., Chen, J., Thompson, J. A., Burbank, D. W., and Yang, H.: Hinge-migrated
1018 fold-scarp model based on an analysis of bed geometry: A study from the Mingyaole
1019 anticline, southern foreland of Chinese Tian Shan, *Journal of Geophysical Research:*
1020 *Solid Earth*, 120, 6592–6613, <https://doi.org/10.1002/2015JB012102>, 2015.
- 1021 Lipparini, L., Chiacchieri, D., Bencini, R., and Micallef, A.: Extensive freshened ground-
1022 water resources emplaced during the Messinian sea-level drawdown in southern Sicily,
1023 Italy, *Communications Earth & Environment*, 4, 430, [https://doi.org/10.1038/s43247-](https://doi.org/10.1038/s43247-023-01077-w)
1024 023-01077-w, 2023.
- 1025 Maesano, F. E., Tiberti, M. M., and Basili, R.: The Calabrian Arc: three-dimensional
1026 modelling of the subduction interface, *Scientific Reports*, 7, 8887, [https://doi.org/](https://doi.org/10.1038/s41598-017-09074-8)
1027 10.1038/s41598-017-09074-8, 2017.
- 1028 Maesano, F. E., Tiberti, M. M., and Basili, R.: Deformation and fault propagation at the
1029 lateral termination of a subduction zone: the Alfeo Fault System in the Calabrian Arc,
1030 southern Italy, *Frontiers in Earth Science*, 8, 107, 2020.
- 1031 Masson, C., Mazzotti, S., and Vernant, P.: Precision of continuous GPS velocities from
1032 statistical analysis of synthetic time series, *Solid Earth*, 10, 329–342, [https://doi.org/](https://doi.org/10.5194/se-10-329-2019)
1033 10.5194/se-10-329-2019, 2019.

- 1034 Mastrolemo, B., Serpelloni, E., Argnani, A., Bonforte, A., Burgmann, R., Anzidei,
1035 M., Baldi, P., and Puglisi, G.: Fast geodetic strain-rates in eastern Sicily (south-
1036 ern Italy): New insights into block tectonics and seismic potential in the area of
1037 the great 1693 earthquake, *Earth and Planetary Science Letters*, 404, [https://doi.org/](https://doi.org/10.1016/j.epsl.2014.07.025)
1038 [10.1016/j.epsl.2014.07.025](https://doi.org/10.1016/j.epsl.2014.07.025), 2014.
- 1039 Mattia, M., Bruno, V., Cannavò, F., and Palano, M.: Evidences of a contractional pattern
1040 along the northern rim of the Hyblean Plateau (Sicily, Italy) from GPS data, *Geologica*
1041 *Acta: an international earth science journal*, 10, 1–8, 2012.
- 1042 Mazzotti, S., James, T. S., Henton, J., and Adams, J.: GPS crustal strain, postglacial
1043 rebound, and seismic hazard in eastern North America: The Saint Lawrence valley ex-
1044 ample: CRUSTAL STRAIN IN SAINT LAWRENCE VALLEY, *Journal of Geophysical*
1045 *Research: Solid Earth*, 110, <https://doi.org/10.1029/2004JB003590>, 2005.
- 1046 Meschis, M., Scicchitano, G., Roberts, G. P., Robertson, J., Barreca, G., Monaco, C.,
1047 Spampinato, C., Sahy, D., Antonioli, F., Mildon, Z. K., and Scardino, G.: Regional De-
1048 formation and Offshore Crustal Local Faulting as Combined Processes to Explain Uplift
1049 Through Time Constrained by Investigating Differentially Uplifted Late Quaternary Pa-
1050 leoshorelines: The Foreland Hyblean Plateau, SE Sicily, *Tectonics*, 39, e2020TC006187,
1051 <https://doi.org/10.1029/2020TC006187>, 2020.
- 1052 Michael, A. J.: Determination of stress from slip data: Faults and folds, *Journal of Geo-*
1053 *physical Research: Solid Earth*, 89, <https://doi.org/10.1029/JB089iB13p11517>, 1984.
- 1054 Milano, M., Kelemework, Y., La Manna, M., Fedi, M., Montanari, D., and Iorio, M.:
1055 Crustal structure of Sicily from modelling of gravity and magnetic anomalies, *Scientific*
1056 *Reports*, 10, 16019, 2020.
- 1057 Minelli, L. and Faccenna, C.: Evolution of the Calabrian accretionary wedge (central
1058 Mediterranean): CALABRIAN ACCRETIONARY WEDGE, *Tectonics*, 29, n/a–n/a,
1059 <https://doi.org/10.1029/2009TC002562>, 2010.
- 1060 Mogi, K.: Relations between the eruptions of various volcanoes and the deformations of
1061 the ground surfaces around them, *Earthquake Research Institute*, 36, 99–134, 1958.
- 1062 Monaco, C. and Tortorici, L.: Active faulting in the Calabrian
1063 arc and eastern Sicily, *Journal of Geodynamics*, 29, 407–424,
1064 <https://www.sciencedirect.com/science/article/pii/S0264370799000526>,
1065 2000.
- 1066 Palano, M., Ferranti, L., Monaco, C., Mattia, M., Aloisi, M., Bruno, V., Cannavò,
1067 F., and Siligato, G.: GPS velocity and strain fields in Sicily and southern Cal-
1068 abria, Italy: Updated geodetic constraints on tectonic block interaction in the central
1069 Mediterranean, *Journal of Geophysical Research: Solid Earth*, 117, [https://doi.org/](https://doi.org/10.1029/2012JB009254)
1070 [10.1029/2012JB009254](https://doi.org/10.1029/2012JB009254), 2012.
- 1071 Prada, M., Sallarès, V., Ranero, C. R., Vendrell, M. G., Grevemeyer, I., Zitellini, N.,
1072 and de Franco, R.: A cross-section of crustal domains and tectonic structure across the
1073 Central Tyrrhenian Basin: from back-arc extension to mantle exhumation, in: *EGU*
1074 *General Assembly Conference Abstracts*, p. 9844, 2014.
- 1075 Rosenbaum, G., Lister, G. S., and Duboz, C.: Reconstruction of the tectonic evolution of
1076 the western Mediterranean since the Oligocene, *Journal of the Virtual Explorer*, 2002.
- 1077 Rovida, A., Locati, M., Camassi, R., Lolli, B., Gasperini, P., and Antonucci, A.:
1078 *Catalogo Parametrico dei Terremoti Italiani (CPTI15)*, versione 4.0, [https://doi.org/](https://doi.org/10.13127/CPTI/CPTI15.4)
1079 [10.13127/CPTI/CPTI15.4](https://doi.org/10.13127/CPTI/CPTI15.4), 2022.

- 1080 Sapin, F., Ringenbach, J.-C., and Clerc, C.: Rifted margins classification and forcing
1081 parameters, *Scientific Reports*, 11, 8199, <https://doi.org/10.1038/s41598-021-87648-3>,
1082 2021.
- 1083 Scandone, P., Patacca, E., Radoicic, R., Ryan, W. B. F., Cita, M. B., Rawson, M., Chezar,
1084 H., Miller, E., McKenzie, J., and Rossi, S.: Mesozoic and Cenozoic rocks from Malta
1085 escarpment (central Mediterranean), *AAPG Bulletin*, 65, 1299–1319, 1981.
- 1086 Scarfi, L., Barberi, G., Barreca, G., Cannavò, F., Koulakov, I., and Patanè, D.: Slab
1087 narrowing in the Central Mediterranean: the Calabro-Ionian subduction zone as imaged
1088 by high resolution seismic tomography, *Scientific Reports*, 8, 5178, <https://doi.org/10.1038/s41598-018-23543-8>, 2018.
- 1090 Schmincke, H.-U., Behncke, B., Grasso, M., and Raffi, S.: Evolution of the northwestern
1091 Iblean Mountains, Sicily: uplift, Pliocene/Pleistocene sea-level changes, paleoenviron-
1092 ment, and volcanism, *Geologische Rundschau*, 86, 637–669, 1997.
- 1093 Scicchitano, G., Antonioli, F., Berlinghieri, E. F. C., Dutton, A., and Monaco, C.: Sub-
1094 merged archaeological sites along the Ionian coast of southeastern Sicily (Italy) and
1095 implications for the Holocene relative sea-level change, *Quaternary Research*, 70, 26–
1096 39, <https://doi.org/10.1016/j.yqres.2008.03.008>, 2008.
- 1097 Scicchitano, G., Gambino, S., Scardino, G., Barreca, G., Gross, F., Mastronuzzi, G., and
1098 Monaco, C.: The enigmatic 1693 AD tsunami in the eastern Mediterranean Sea: new
1099 insights on the triggering mechanisms and propagation dynamics, *Scientific Reports*,
1100 12, 9573, <https://doi.org/10.1038/s41598-022-13538-x>, 2022.
- 1101 Scognamiglio, L., Tinti, E., and Quintiliani, M.: Time Domain Moment Tensor (TDMT),
1102 <https://doi.org/10.13127/TDMT>, 2006.
- 1103 Sgroi, T., de Nardis, R., and Lavecchia, G.: Crustal structure and seis-
1104 motectonics of central Sicily (southern Italy): new constraints from in-
1105 strumental seismicity, *Geophysical Journal International*, 189, 1237–1252,
1106 <https://academic.oup.com/gji/article-abstract/189/3/1237/608535>, 2012.
- 1107 Silverii, F., D’Agostino, N., Métois, M., Fiorillo, F., and Ventafridda, G.: Transient
1108 deformation of karst aquifers due to seasonal and multiyear groundwater variations
1109 observed by GPS in southern Apennines (Italy), *Journal of Geophysical Research: Solid
1110 Earth*, 121, 8315–8337, <https://doi.org/10.1002/2016JB013361>, 2016.
- 1111 S.I.T.R. regione Siciliana: Scheda metadato DATASET Mod-
1112 ello digitale del terreno (MDT) 2m - Volo ATA 2012 2013
1113 - Regione Siciliana - S.I.T.R. Infrastruttura Dati Territoriali,
1114 <https://www.sitr.regione.sicilia.it/geoportale/it/metadata/details/946>,
1115 2013.
- 1116 Spampinato, C. R., Braitenberg, C., Monaco, C., and Scicchitano, G.: Analysis of verti-
1117 cal movements in eastern Sicily and southern Calabria (Italy) through geodetic level-
1118 ing data, *Journal of Geodynamics*, 66, 1–12, <https://doi.org/10.1016/j.jog.2012.12.002>,
1119 2013.
- 1120 Speranza, F., Minelli, L., Pignatelli, A., and Chiappini, M.: The Ionian Sea: The oldest
1121 in situ ocean fragment of the world?: MAGNETIC MODELLING OF THE IONIAN
1122 SEA, *Journal of Geophysical Research: Solid Earth*, 117, n/a–n/a, <https://doi.org/10.1029/2012JB009475>, 2012.
- 1124 Stampfli, G., Borel, G., Marchant, R., and Mosar, J.: Western Alps geological con-

- 1125 straints on western Tethyan reconstructions, *Journal of the Virtual Explorer*, 08,
1126 <https://doi.org/10.3809/jvirtex.2002.00057>, 2002.
- 1127 Stephenson, O. L., Liu, Y.-K., Yunjun, Z., Simons, M., Rosen, P., and Xu, X.: The Im-
1128 pact of Plate Motions on Long-Wavelength InSAR-Derived Velocity Fields, *Geophysical*
1129 *Research Letters*, 49, e2022GL099835, <https://doi.org/10.1029/2022GL099835>, 2022.
- 1130 Tesauro, M., Audet, P., Kaban, M. K., Bürgmann, R., and Cloetingh, S.: The effective
1131 elastic thickness of the continental lithosphere: Comparison between rheological and
1132 inverse approaches: *Te OF THE CONTINENTAL LITHOSPHERE*, *Geochemistry,*
1133 *Geophysics, Geosystems*, 13, <https://doi.org/10.1029/2012GC004162>, 2012.
- 1134 Toda, S., Stein, R. S., Sevilgen, V., and Lin, J.: Coulomb 3.3 Graphic-rich deformation
1135 and stress-change software for earthquake, tectonic, and volcano research and teach-
1136 ing—user guide, US Geological Survey open-file report, 1060, 63, 2011.
- 1137 Trua, T., Serri, G., and Marani, M. P.: Lateral flow of African mantle below the nearby
1138 Tyrrhenian plate: geochemical evidence, *Terra Nova*, 15, 433–440, <https://doi.org/10.1046/j.1365-3121.2003.00509.x>, 2003.
- 1140 Tugend, J., Chamot-Rooke, N., Arsenikos, S., Blanpied, C., and Frizon De Lamotte,
1141 D.: *Geology of the Ionian Basin and Margins: A Key to the East Mediterranean*
1142 *Geodynamics, Tectonics*, 38, 2668–2702, <https://doi.org/10.1029/2018TC005472>, 2019.
- 1143 Turcotte, D. L. and Schubert, G.: *Geodynamics*, Cambridge University Press, Cambridge,
1144 United Kingdom, third edition edn., ISBN 978-1-107-00653-9 978-0-521-18623-0, 2014.
- 1145 Van Hinsbergen, D. J., Torsvik, T. H., Schmid, S. M., Mañenco, L. C., Maffione, M.,
1146 Vissers, R. L., Gürer, D., and Spakman, W.: Orogenic architecture of the Mediter-
1147 ranean region and kinematic reconstruction of its tectonic evolution since the Triassic,
1148 *Gondwana Research*, 81, 79–229, <https://doi.org/10.1016/j.gr.2019.07.009>, 2020.
- 1149 Vavryčuk, V.: Iterative joint inversion for stress and fault orientations from fo-
1150 cal mechanisms, *Geophysical Journal International*, 199, 69–77, <https://doi.org/10.1093/gji/ggu224>, 2014.
- 1152 ViDEPI: Progetto ViDEPI-Visibilità dei Dati Afferenti All’Attività di Esplorazione Petro-
1153 lifera in Italia. 2016 (Last Upgrade).
- 1154 Vilardo, G., Ventura, G., Terranova, C., Matano, F., and Nardò, S.: Ground deformation
1155 due to tectonic, hydrothermal, gravity, hydrogeological, and anthropic processes in
1156 the Campania Region (Southern Italy) from Permanent Scatterers Synthetic Aperture
1157 Radar Interferometry, *Remote Sensing of Environment*, 113, 197–212, <https://doi.org/10.1016/j.rse.2008.09.007>, 2009.
- 1159 Vollrath, A., Zucca, F., Bekaert, D., Bonforte, A., Guglielmino, F., Hooper, A., and
1160 Stramondo, S.: Decomposing DInSAR Time-Series into 3-D in Combination with GPS
1161 in the Case of Low Strain Rates: An Application to the Hyblean Plateau, Sicily, Italy,
1162 *Remote Sensing*, 9, 33, <https://doi.org/10.3390/rs9010033>, 2017.
- 1163 Watts, A. B. and Zhong, S.: Observations of $\bar{\epsilon}$ -exure and the rheology of oceanic litho-
1164 sphere, 2000.
- 1165 Wells, D. L. and Coppersmith, K. J.: New empirical relationships among
1166 magnitude, rupture length, rupture width, rupture area, and surface dis-
1167 placement, *Bulletin of the seismological Society of America*, 84, 974–1002,
1168 <https://pubs.geoscienceworld.org/ssa/bssa/article-abstract/84/4/974/119792>,
1169 1994.

- 1170 Wessel, P. and Smith, W. H. F.: New, improved version of generic mapping tools re-
1171 leased, *Eos, Transactions American Geophysical Union*, 79, 579–579, [https://doi.org/](https://doi.org/10.1029/98EO00426)
1172 [10.1029/98EO00426](https://doi.org/10.1029/98EO00426), 1998.
- 1173 White, A. M., Gardner, W. P., Borsa, A. A., Argus, D. F., and Martens,
1174 H. R.: A Review of GNSS/GPS in Hydrogeodesy: Hydrologic Loading Appli-
1175 cations and Their Implications for Water Resource Research, *Water Resources*
1176 *Research*, 58, e2022WR032078, <https://doi.org/10.1029/2022WR032078>, _eprint:
1177 <https://onlinelibrary.wiley.com/doi/pdf/10.1029/2022WR032078>, 2022.
- 1178 Wickert, A. D.: Open-source modular solutions for flexural isostasy: gFlex v1.0, *Geo-*
1179 *scientific Model Development*, 9, 997–1017, <https://doi.org/10.5194/gmd-9-997-2016>,
1180 2016.
- 1181 Wortel, M. J. R. and Spakman, W.: Subduction and Slab Detachment in
1182 the Mediterranean-Carpathian Region, *Science*, 290, 1910–1917, [https://doi.org/](https://doi.org/10.1126/science.290.5498.1910)
1183 [10.1126/science.290.5498.1910](https://doi.org/10.1126/science.290.5498.1910), 2000.
- 1184 Zitellini, N., Ranero, C. R., Loreto, M. F., Ligi, M., Pastore, M., D’Oriano, F., Sallares,
1185 V., Grevemeyer, I., Moeller, S., and Prada, M.: Recent inversion of the Tyrrhenian
1186 Basin, *Geology*, 48, 123–127, <https://doi.org/10.1130/G46774.1>, 2020.